Shell chemistry of the Boreal Campanian bivalve *Rastellum diluvianum* (Linnaeus, 1767) reveals temperature seasonality, growth rates and life cycle of an extinct Cretaceous oyster.

Niels J. de Winter[1], Clemens V. Ullmann[2], Anne M. Sørensen[3], Nicolas Thibault[4], Steven Goderis[1], Stijn J.M. Van Malderen[5], Christophe Snoeck[1,6], Stijn Goolaerts[7], Frank Vanhaecke[5], Philippe Claeys[1]

[1]AMGC research group, Vrije Universiteit Brussel, Pleinlaan 2, B-1050 Brussels, Belgium.

[2]Camborne School of Mines, University of Exeter, Penryn, Cornwall, TR10 9FE, UK.

[3]Trap Danmark, Agem All 13, DK-2970, Hørsholm, Denmark.

[4] Department of Geoscience and Natural Resource Management, University of Copenhagen, Øster Voldgade 10, DK-1350 Copenhagen C., Denmark.

[5]A&MS research unit, Ghent University Campus Sterre, Krijgslaan 281, Building S12, B-9000 Ghent, Belgium.

[6]G-Time laboratory, Université Libre de Bruxelles, 50 Avenue F.D. Roosevelt, B-1050, Brussels, Belgium.

[7]Directorate of Earth and History of Life, Royal Belgian Institute of Natural Sciences, Vautierstraat 29, B-1000 Brussels, Belgium.

Correspondence to: Niels J. de Winter (niels.de.winter@vub.be)

Abstract

The Campanian age (Late Cretaceous) is characterized by a warm greenhouse climate with limited land ice volume. This makes this period an ideal target for studying climate dynamics during greenhouse periods, which are essential for predictions of future climate change due to anthropogenic greenhouse gas emissions. Well-preserved fossil shells from the Campanian (±78 Ma) high mid-latitude (50°N) coastal faunas of the Kristianstad Basin (southern Sweden) offer a unique snapshot of short-term climate and environmental variability, which complement existing long-term climate reconstructions. In this study, we apply a combination of high-resolution spatially resolved trace element analyses (µXRF and LA-ICP-MS), stable isotope analyses (IRMS) and growth modelling to study short-term (seasonal) variations recorded in the oyster species *Rastellum diluvianum* from the Ivö Klack locality. Geochemical records through 12 specimens shed light on the influence of specimen-specific and ontogenetic effects on the expression of seasonal variations in shell chemistry and allows disentangling vital effects from environmental influences in an effort to refine palaeoseasonality reconstructions of Late Cretaceous greenhouse climates. Growth models based on stable oxygen isotope records yield information on the mode of life, circadian rhythm and reproductive cycle of these extinct oysters. This multi-proxy study reveals that mean annual temperatures in the Campanian higher mid-latitudes were 17 to 19°C with winter minima of ~13°C and summer maxima of 26°C, assuming a Late Cretaceous seawater oxygen isotope composition of -1‰VSMOW. These results yield Campanian latitudinal temperature gradients similar to the present, but with smaller latitudinal differences in temperature seasonality, contrasting with previous notions of “equable climate” during the Late Cretaceous. Our results also demonstrate that species-specific differences and uncertainties in the composition of Late Cretaceous seawater prevent trace element proxies (Mg/Ca, Sr/Ca, Mg/Li and Sr/Li) to be used as reliable temperature proxies for fossil oyster shells. However, trace element profiles can serve as a quick tool for diagenesis screening and investigating seasonal growth patterns in ancient shells.

1. Introduction

The Late Cretaceous was marked by a long cooling trend that brought global mean annual temperatures (MAT) down from the mid-Cretaceous climate maximum (±28°C surface ocean temperatures) in the

Cenomanian and Turonian (±95 Ma) to slightly cooler temperatures (±22°C surface ocean temperatures) around the Campanian-Maastrichtian boundary (±72.1 Ma; Clarke and Jenkyns, 1999; Pearson et al., 2001; Huber et al., 2002; Friedrich et al., 2012; Scotese, 2016). This cooling trend was likely caused by a change in ocean circulation, initiated by the opening of the Equatorial Atlantic Gateway that separated the proto-North and -South Atlantic Ocean basins (Friedrich et al., 2009). The cooling trend is well documented in stable oxygen isotope records from the white chalk successions of the Chalk Sea, which covered large portions of northwestern Europe during the Late Cretaceous Period (Reid, 1973; Jenkyns et al., 1994; Jarvis et al., 2002; Voigt et al., 2010). The connection of the Chalk Sea to the (proto-)North Atlantic Ocean makes it an interesting area of study to constrain Late Cretaceous paleogeography and climate. These chalk successions featured in various paleoclimate studies, because they are accessible in good outcrops and consist predominantly of calcareous nannofossils which were thought to faithfully record sea surface conditions (e.g. Jenkyns et al., 1994). However, recent studies (e.g. O'Brien et al., 2017; Tagliavento et al., 2019) have shown that diagenetic overprinting likely biases these records towards cooler temperatures, resulting in the apparent Cool Tropics Paradox (Pearson et al., 2001). Even though sea level changes seem to indicate possible small changes in land ice volume during the Late Cretaceous, warm high-latitude paleotemperatures likely rule out the possibility of extensive polar ice sheets comparable in volume to modern ice caps (Barrera and Johnson, 1999; Huber et al., 2002; Jenkyns et al., 2004; Miller et al., 2005; Thibault et al., 2016).

Given its warm, land ice free conditions, the Campanian serves as an interesting analogue for Earth's climate in the future, should anthropogenic and natural emissions continue to contribute to the rise in global temperatures and decrease global ice volume on Earth (IPCC, 2013; Donnadieu et al., 2016). However, most Late Cretaceous climate reconstructions focus on reconstructing and modelling long-term evolutions of humid/arid conditions on land or past atmospheric and oceanic temperatures (DeConto et al., 1999; Thibault et al., 2016; Yang et al., 2018). Data on the extent of seasonal variability from this time period, especially outside the tropics, are scarce, although seasonality constitutes a fundamental component of the climate system (Steuber, 1999; Steuber et al., 2005; Burgener et al., 2018). Furthermore, many proxies used for paleoclimate reconstruction risk being seasonally biased, and thus independent seasonality reconstructions serve as important tools to verify other climate reconstructions.

2. Background

2.1 Geological setting

The Kristianstad Basin, our study site, is located on the southeastern Baltic Sea coast of the southern Swedish province of Skåne, which is presently located at 56°2' N, 14° 9' E (see **Fig. 1**), somewhat higher than its Campanian paleolatitude, which is estimated at 50°N (van Hinsbergen et al., 2015). The uppermost lower Campanian shallow marine sediments deposited at Ivö Klack consist of sandy and silty nearshore deposits containing carbonate gravel (Christensen, 1975; 1984; Surlyk and Sørensen, 2010; Sørensen et al., 2015). The depositional setting is described as a rocky coastline that was inundated during the maximum extent of the Late Cretaceous transgression (Kominz et al., 2008; Csiki-Sava et al., 2015). Since the region has remained tectonically quiet since the Campanian, the deposits of Kristianstad Basin localities remain at roughly the same altitude as when they were deposited and have been subject to limited burial (Christensen, 1984; Surlyk and Sørensen, 2010).

The rocky shore deposits of Ivö Klack are characterized by a diverse shelly fauna, consisting of well-preserved fossils and fragments of brachiopods, belemnites, echinoids and asteroids, polychaete worms, gastropods, corals, ammonites and thick-shelled oysters, with a total of almost 200 different recognized species (Surlyk and Sørensen, 2010). In this diverse rocky shore ecosystem, various habitat zones can be distinguished, each with their distinct suite of organisms adapted to local conditions of varying amounts of sunlight, sedimentation and turbulence (Surlyk and Christensen, 1974; Sørensen et al., 2012). This unique combination of marine biodiversity and preservation of original calcite shell material makes the localities in the Kristianstad Basin ideal for studying sub-annual variability in shell chemistry and reconstructing paleoseasonality and environmental change in the Campanian (Sørensen et al., 2015).

2.2 Bivalve shells

Fossil bivalve shells offer a valuable archive for studying past climates on a seasonal scale. Incremental measurements of shell chemistry in growth direction (sclerochronology studies) potentially yield records of seasonal changes in the environment (Mook, 1971; Jones, 1983; Klein et al., 1996; Schöne and Gillikin, 2013). Their distribution allows paleoseasonality reconstructions from bivalves across a wide range of

latitudes (Roy et al., 2000; Jablonski et al., 2017), and the preservation potential of calcitic shell structures (especially in oyster shells) makes them ideal, if not unique, recorders of pre-Quarternary seasonality and sub-annual environmental change (Brand and Veizer, 1980; 1981; Al-Aasm and Veizer, 1986a; b; Immenhauser et al., 2005; Alberti et al., 2017). The incremental deposition of shell carbonate means, in theory, that the limits in terms of time resolution of the bivalve shell archive are governed by sampling resolution rather than the resolution of the record itself. While periods of growth cessation can occur (especially in high latitudes, Ullmann et al., 2010) and the true mechanisms of shell deposition on a very high (e.g. daily) temporal resolution are poorly constrained (see de Winter et al., 2020a and references therein), in practice incremental shell deposition allows reconstructions of changes down to sub-daily timescales given the right sampling techniques (Schöne et al., 2005; Sano et al., 2012; Warter et al., 2018; de Winter et al., 2020a). Examples of chemical proxies used in such sclerochronology studies include stable carbon and oxygen isotope ratios and trace element ratios (e.g. Steuber et al., 2005; Gillikin et al., 2006; McConnaughey and Gillikin, 2008; Schöne et al., 2011; de Winter et al., 2017a; 2018).

2.3 Trace element proxies

The incorporation of trace elements and carbon isotopes into bivalve shells is influenced by so-called vital effects: biological controls on the incorporation of elements in the shell independent of the environment (Weiner and Dove, 2003; Gillikin et al., 2005). These vital effects have been shown to mask the characteristic relationships between shell trace element chemistry and the environment and appear to be distinct not only between different bivalve species but also between specimens of different ontogenetic age (Freitas et al., 2008). Differences between bivalve families mean that the trace element chemistry of some taxa (like scallops: Family Pectinidae) are especially affected by vital effects (Lorrain et al., 2005; Freitas et al., 2008), while other families like oysters (Family Ostreidae) seem to be more robust recorders of environmental conditions (Surge et al., 2001; Surge and Lohmann, 2008; Ullmann et al., 2010; 2013). The effect on shell composition and preservation of changes in microstructure and the amount of organic matrix present in different shell layers introduces uncertainty as to which parts of the shells are well-suited for reconstruction purposes (Carriker et al., 1991; Kawaguchi et al., 1993; Dalbeck et al., 2006; Schöne et al., 2010; 2013). The key to disentangling these vital effects from recorded environmental changes lies in the application of multiple proxies and techniques on the same bivalve shells (the “multi-proxy approach”; e.g.

Ullmann et al., 2013; de Winter et al., 2017a; 2018) and to base reconstructions on more than one shell (Ivany, 2012).

2.4 Stable isotope ratios

Because nearly all bivalves precipitate their shells at or near oxygen isotope equilibrium, the stable oxygen isotope ratio of bivalve shell carbonate is less susceptible to vital effects, such as growth kinetics (Uchikawa and Zeebe, 2012). Therefore, stable oxygen isotope ratios in bivalve shell carbonate ($\delta^{18}O_c$) are solely dependent on calcification temperature and sea water oxygen isotope composition ($\delta^{18}O_{sw}$), and this proxy is frequently used in sclerochronology studies as a paleothermometer (Kim and O'Neil, 1997; Schöne et al., 2005; Butler et al., 2013; Ullmann et al., 2013; Huyghe et al., 2015; de Winter et al., 2020b). Oxygen isotope records can function as a reference in the above-mentioned multi-proxy studies aimed at resolving vital effects, environmental and climatic changes. However, the weakness of this proxy lies in the fact that $\delta^{18}O_{sw}$ is not always known, especially in deep time settings (Veizer and Prokoph, 2015). As a result, a constant $\delta^{18}O_{sw}$ of 0‰VSMOW for modern icehouse climate conditions, or -1‰VSMOW for an ice-free world (such as the Eocene or the Late Cretaceous; after Shackleton, 1986) is often assumed (e.g. Andreasson and Schmitz, 1996; Ivany and Runnegar, 2010; Huyghe et al., 2015). An offset of 1‰ between assumed $\delta^{18}O_{sw}$ and actual $\delta^{18}O_{sw}$ can result in a ~4.6°C temperature offset in temperature reconstructions (Kim and O'Neil, 1997) This assumption may therefore introduce inaccuracies in absolute temperature reconstructions, but relative variations in $\delta^{18}O_c$ can still yield important insights into high-resolution climate dynamics.

In marine mollusks, dissolved inorganic carbon (DIC) in the ambient sea water contributes the largest fraction of carbon (90%) used for shell mineralization (McConnaughey, 2003; Gillikin et al., 2007) and therefore heavily influences $\delta^{13}C$ values of shell carbonate. However, changes in respiration rates can alter the carbon budget of shell carbonate by adding or removing isotopically light respired carbon in the form of CO_2 (Lorrain et al., 2004). Environmental changes in DIC can also have a strong influence on this carbon budget, especially when bivalves grow in nearshore or estuarine conditions with large (seasonal) variations in environmental $\delta^{13}C$ of DIC and organic carbon (Gillikin et al., 2006). Conceptual models exist that attempt to correlate shell $\delta^{13}C$ in modern mollusks to environmental and physiological variations, but these require

knowledge of ambient CO_2 pressures and $\delta^{13}C$ values of DIC, gas ventilation rates in the animal and CO_2 and O_2 permeabilities of calcifying membranes (McConnaughey et al., 1997), which are not available in fossil bivalve studies.

2.5 Aim In this study, we present a detailed, multi-proxy comparison of the growth and chemistry of well-preserved fossil shells of the thick-shelled oyster *Rastellum diluvianum* (Linnaeus, 1767) recovered from the Ivö Klack locality on the northern edge of the Kristianstad Basin. We combine stable isotope proxies conventional in sclerochronological studies ($\delta^{13}C$ and $\delta^{18}O$; e.g. Goodwin et al., 2001; Steuber et al., 2005) with less well-established trace element proxies (Mg/Ca, Sr/Ca, Mg/Li and Sr/Li; e.g. Bryan and Marchitto, 2008; Schöne et al., 2011; Füllenbach et al., 2015; Dellinger et al., 2018) and growth modelling based on $\delta^{18}O$ seasonality (Judd et al., 2018) in an attempt to disentangle the effects of growth rate, reproductive cycle and environmental change on shell chemistry. The data gathered in this study allow a detailed discussion on seasonal changes in temperature and water chemistry in the coastal waters of the Kristianstad Basin in the late early Campanian, as well as on the life cycle of *R. diluvianum* and its response to seasonal changes in its environment.

175

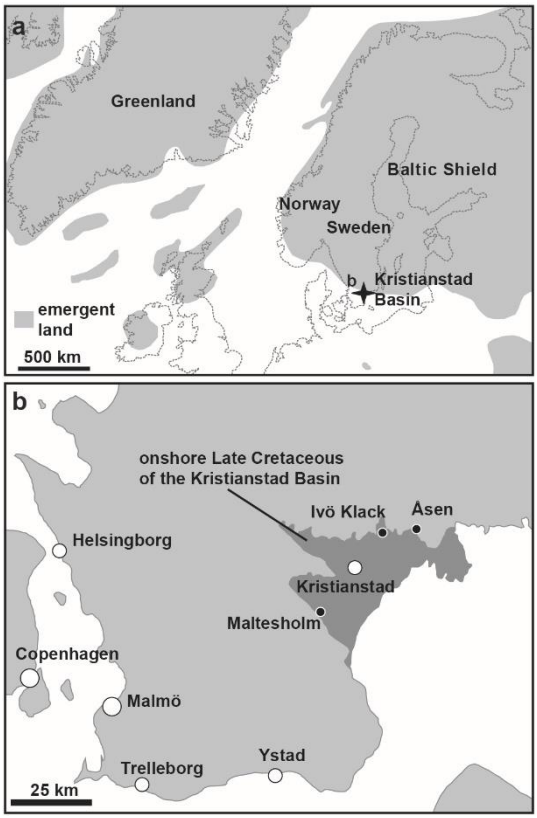

Figure 1: Paleogeographic map of the Boreal Chalk Sea (**a**) and the area of present-day southern Sweden (**b**) showing the location of Ivö klack (modified after Sørensen et al., 2015)

176

3. Materials and Methods

3.1 Sample acquisition and preparation

Complete valves of twelve individual *R. diluvianum* oysters were obtained from the Ivö Klack locality (see **Fig. 2**). Specimens of *R. diluvianum* were found *in situ* attached to the vertical sides of large boulders that characterized the rocky shore of Ivö Klack (Surlyk and Christensen, 1974) and are biostratigraphically assigned to the latest early Campanian *B. mammillatus* belemnite zone. The valves were cleaned and fully embedded in Araldite® 2020 epoxy resin (Bodo Möller Chemie Benelux, Antwerp, Belgium). Dorsoventral slabs (±10 mm thick) were cut perpendicular to the hinge line using a water-cooled slow rotating saw with a diamond-coated blade (thickness ± 1 mm; **Fig. 2**). The surfaces cut on the central growth axis were progressively polished using silicon-carbide polishing disks (up to P2500, or 8.4 µm grain size). Polished surfaces were scanned at high (6400 dpi) resolution using an Epson Perfection 1650 flatbed color scanner (Seiko Epson Corp., Suwa, Japan). Resulting color scans of all polished *R. diluvianum* shell cross sections are provided in **Fig. 2** and **S1**. Shell microstructures in *R. diluvianum* shells were studied in detail on high-resolution scans and by using reflected light optical microscopy. Microstructural features were used to reconstruct the relative timing of shell growth (see **Fig. 3**). Fragments of visually well-preserved material from different microstructures in the shells were coated with gold and studied under a Scanning Electron Microscope (Quanta 200 ESEM) and imaged at 1000x – 2000x magnification (**Fig. 3b-e**). Chemical analyses were carried out sequentially on polished cross sections in order of destructive character of sampling (starting with the least destructive measurements: µXRF, LA-ICP-MS, microdrilling for IRMS and finally MC-ICP-MS analysis on ~26 mg samples).

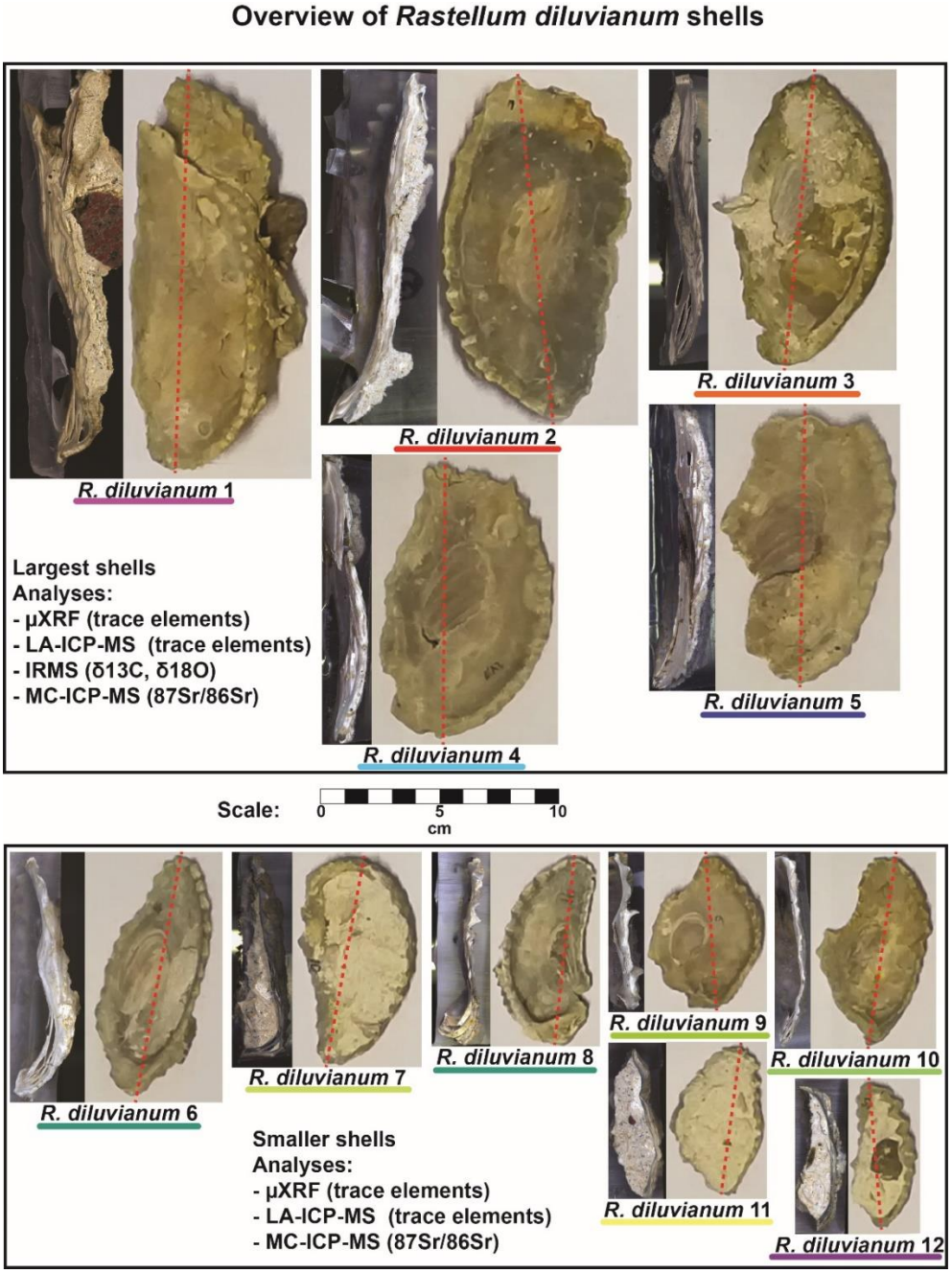

Figure 2: Overview of the 12 *Rastellum diluvianum* shells used in this study. All shells are depicted on the same scale (see scalebar in center of image). Colors of the lines under sample names correspond to the colors of the lines in **Fig. 4**, **Fig. 6**, **Fig. 8** and **Fig. 10**. Every shell is represented by an image of the inside of the valve analyzed, as well as a color scan of the cross section through the shell on which high-resolution analyses were carried out. Dashed red lines show the location of these cross sections. The largest 5 shells (1-5, on top half) were sampled for IRMS analyses ($\delta^{13}C$ and $\delta^{18}O$). All shells were subjected to micro X-ray fluorescence (µXRF), laser ablation inductively coupled plasma mass spectrometry (LA-ICP-MS) and multi-cup inductively coupled plasma mass spectrometry (MC-ICP-MS) analyses. Full-size versions of the high-resolution color scans of shell cross sections are provided in **S1**.

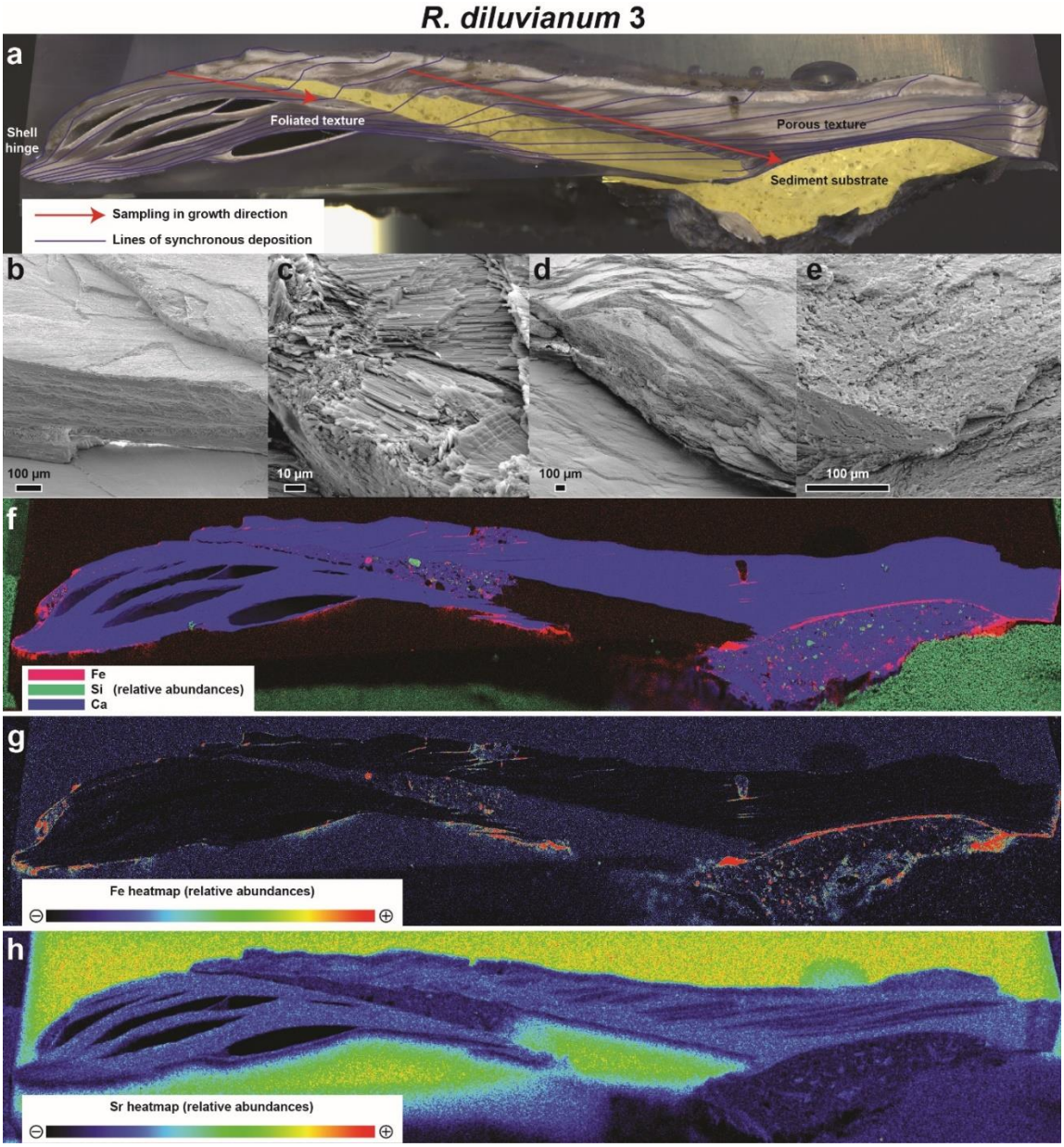

Figure 3: Overview image showing a high-resolution color scan of the cross section through *R. diluvianum* 3 (**a**) on which the different shell textures as well as the directions of high-resolution analyses (in growth direction) are indicated. Thin blue lines denote parts of the shell that were deposited at the same time (growth increments). Areas marked in yellow represent sediment infilling below and between the valves. (**b**) and (**c**) show SEM images of the well-preserved foliated calcite in the shell. More porous structures in the shell (vesicular calcite) are depicted in SEM images shown in (**d**) and (**e**). Below are shown three XRF elemental maps of the same cross section: An RGB-colored map displaying the relative abundances of Fe, Si and Ca (**f**), A heatmap of Fe concentrations (**g**; see scalebar below map) and a heatmap of Sr concentrations (**h**; see scalebar below map). XRF mapping only yields relative (semi-quantitative) abundance of elements.

3.2 Micro-XRF mapping

Elemental abundance maps of all *R. diluvianum* shell cross sections were obtained using a Bruker Tornado M4 energy-dispersive micro-X-Ray Fluorescence scanner (µXRF; Bruker nano GmbH, Berlin, Germany) All µXRF analyses carried out with the Bruker M4 Tornado are non-destructive. The µXRF is equipped with a Rh filament metal-ceramic tube X-Ray source operated at 50 kV and 600 µA (30 W; maximum energy settings). The circular spot projected on the same surface is estimated to have a diameter of 25 µm (Mo-Kα). A µm-precision XYZ translation stage allows for quick and precise sample movement such that a grid of 25 µm XRF spots can be measured on the sample surface by continuous scanning to construct elemental maps ($3 * 10^6$ - $5 * 10^6$ pixels per map). Exposure times of the X-ray beam per sampling position in mapping mode (1 ms/pixel) are too short to gain adequate signal-to-noise ratio for pixel-by-pixel quantification of elemental concentrations. Instead, processing of entire map surfaces using the Bruker Esprit™ software allows semi-quantitative elemental abundance maps to be created of the sample surface based on a mapping of the count rate in Regions of Interest of elements (see de Winter and Claeys, 2016; de Winter et al., 2017b; **Fig. 3**). XRF maps allow for a rapid assessment of the preservation state of original shell calcite based on variations in Si, Mn, Fe and Sr concentrations and guide the selection of sampling protocols for further analyses (de Winter and Claeys, 2016; **Fig. 3**). Results of XRF mapping on all 12 *R. diluvianum* shell cross sections are provided in **S2**.

3.3 Micro-XRF line scans

After XRF mapping, quantitative line scans were measured in growth direction on shell cross sections. Dwell times of 60 seconds per measurement yielded sufficiently high signal-to-noise ratios for individual points in line scans to be quantified. This acquisition time was chosen as to provide the optimal compromise between increasing run time (improved signal/noise ratio; enhanced reproducibility) and increasing the number of sampling positions (improving sampling density and allowing duplicate measurements) for the elements Mg, Al, Si, P, S, Ca, Ti, Mn, Fe, Cu, Zn and Sr (see discussion in de Winter et al., 2017b). The sampling interval of line scans was 50 µm, adding up to a total of 11056 individual quantitative XRF spectra measured for this study. Spectra were quantified using the Bruker Esprit software calibrated using the matrix-matched BAS-CRM393 limestone standard (Bureau of Analyzed samples, Middlesbrough, UK), after

which individual measurements were calibrated offline using 7 matrix-matched certified reference materials (CCH1, COQ1, CRM393, CRM512, CRM513, ECRM782 and SRM1d), which were treated as samples (see Vansteenberge et al., 2020). R^2 values of calibration curves exceeded 0.99 and reproducibility standard deviations were better than 10% relative to the mean. Even though line scans were positioned on well-preserved shell calcite based on the XRF map results, a second check was carried out in which individual points were rejected based on conservative thresholds for diagenetic recrystallization or detrital contamination ([Ca] < 38 wt%, [Si] > 1 wt%, [Mn] > 200 µg/g or [Fe] > 250 µg/g; [Sr]/[Mn] < 100 mol/mol; see Al-Aasm and Veizer, 1986a; Sørensen et al., 2015). Concentrations of Ca, Mg and Sr in well-preserved shell sections were used to explore the potential of Mg/Ca and Sr/Ca molar ratios as paleoenvironmental proxies. Unprocessed results of XRF line scanning are provided in **S3**.

3.4 LA-ICP-MS line scans

Spatially resolved elemental concentrations for Li, B, Mg, Si, P, Ca, Ti, V, Cr, Mn, Fe, Ni, Zn, Rb, Sr, Ba, Pb and U were calculated from a calibrated transient MS signal recorded during Laser Ablation-Inductively Coupled Plasma-Mass Spectrometry (LA-ICP-MS) line scanning in the growth direction (parallel to the XRF line scans) on shell cross sections. LA-ICP-MS measurements were carried out at the Atomic and Mass Spectrometry – A&MS research unit of Ghent University (Ghent, Belgium) using a 193 nm ArF*excimer-based Analyte G2 laser ablation system (Teledyne Photon Machines, Bozeman, USA), equipped with a HelEx 2 double-volume ablation cell, coupled to an Agilent 7900 quadrupole-based ICP-MS unit (Agilent, Tokyo, Japan). Continuous scanning along shell transects using a laser spot with a diameter of 25 µm, scan speed of 50 µm/s and detector mass sweep time of 0.5 s yielded profiles with a lateral sampling interval of 25 µm, amounting to a total of 9505 LA-ICP-MS data points gathered. The aerosol was transported using He carrier gas into the ICP-MS unit via the aerosol rapid introduction system (ARIS; Teledyne Photon Machines, Bozeman, USA). Elemental concentrations were calibrated using bracketed analysis runs on US Geological Survey (USGS) BCR-2G, BHVO-2G, BIR-1G, GSD-1G and GSE-1G and National Institute of Standards and Technology (NIST) SRM612 and SRM610 certified reference materials. Calcium concentrations (measured via ^{43}Ca) were used as internal standard for data normalization and drift correction during the measurement campaign, and Ca concentrations of 38.5 wt% were assumed for pristine shell carbonate. Coefficients of determination (R^2) of a linear model fitted to the calibration curves

were better than 0.99 and the standard deviation of reproducibility for elemental concentrations was better than 5% relative to the mean value. Individual LA-ICP-MS measurements were inspected for diagenetic alteration or contamination by detrital material using the same thresholds as used for XRF data (see above). LA-ICP-MS and µXRF measurements were combined to cover a wider range of elements, since some elements (e.g. S and Sr) were measured more reliably using µXRF, while others (e.g. Li or Ba) could only be quantified using LA-ICP-MS. Concentrations of Li, Mg, and Sr were used to explore the potential of Mg/Li and Sr/Li molar ratios as proxies for paleoenvironmental change. Unprocessed results of LA-ICP-MS line scans are provided in **S4**.

3.5 Isotope Ratio Mass Spectrometry

A transect of powdered samples (±200 µg) was sampled for Isotope Ratio Mass Spectrometry (IRMS) analysis in growth direction along well-preserved foliated calcite (**Fig. 3**) in the five largest of the twelve *R. diluvianum* shells (*R. diluvianum* 1-5; see **Fig. 2**) using a microdrill (Merchantek/Electro Scientific Industries Inc., Portland (OR), USA) equipped with a 300 µm diameter tungsten carbide drill bit, coupled to a microscope (Leica GZ6, Leica Microsystems GmbH, Wetzlar, Germany). A total of 531 IRMS samples were taken at an interspacing of 250 µm. Stable carbon and oxygen isotope ratios ($\delta^{13}C$ and $\delta^{18}O$) were measured in a NuPerspective IRMS equipped with a NuCarb carbonate preparation device (Nu Instruments, UK). The sample size (50-100 µg) allowed duplicate measurements to be carried out regularly (roughly once every 30 samples) to assess reproducibility. Samples were digested in 104% phosphoric acid at a constant temperature of 70°C and the resulting CO_2 gas was cryogenically purified before being led into the IRMS through a dual inlet system. Isotope ratios were corrected for instrumental drift and fractionation due to variations in sample size and the resulting values are reported relative to the Vienna Pee Dee Belemnite standard (‰VPDB) using repeated measurements of the IA-603 stable isotope standard (International Atomic Energy Agency, Vienna, Austria). Reproducibility of $\delta^{18}O$ and $\delta^{13}C$ measurements on this standard were better than 0.1‰ and 0.05‰ (1σ; N=125) respectively. All stable isotope analysis results are provided in **S5** and plots of stable isotope and trace element records from all shells are given in **S6**.

3.6 Growth and age modelling

Stable oxygen isotope curves measured in *R. diluvianum* were used to produce age models for the growth of the shell using a bivalve growth model written in MatLab (Mathworks, Natick, MA, USA) which simulates $\delta^{18}O$ curves using a combination of growth and temperature sinusoids (Judd et al., 2018). This simulation model was modified to calculate its temperatures based on calcite $\delta^{18}O$ (following Kim and O'Neil, 1997) rather than from the aragonite $\delta^{18}O$-temperature relationship used in the original approach (after Grossman and Ku, 1986; see Judd et al., 2018). A value of -1.0‰ VSMOW was assumed for $\delta^{18}O$ of Campanian ocean water (Shackleton, 1986; Thibault et al., 2016). Additional minor modifications in the source code allowed results of intermediate calculation steps in the model to be exported. The modified Matlab source code is provided in **S7**. Note that this model assumes that the shape and absolute value of $\delta^{18}O$ curves depend solely on water temperature and growth rate (ignoring changes in $\delta^{18}O_{sw}$), and that a modelled year contains 365 days by construction (while this number should be slightly larger in the Late Cretaceous; de Winter et al., 2020a). Despite these caveats, shell chronologies reconstructed from seasonal patterns in $\delta^{18}O$ should still be reliable as they are only based on the shape of the $\delta^{18}O$ curves. Uncertainties on modelled temperature curves were derived by propagating the measurement uncertainty on $\delta^{18}O$. Age models thus obtained for shells *R. diluvianum* 1-5 were used to align all proxy records on a common time axis. Age models for *R.diluvianum* 6-12 were constructed by extrapolating relationships between modelled seasonality and microstructures and trace element concentrations observed in *R. diluvianum* 1-5. Simultaneously deposited microstructural features in shell cross sections (see **Fig. 3**) were used to determine the actual dorsoventral height of the shells at different ages, linking shell height to the age and allowing the construction of growth curves for all twelve *R. diluvianum* shells. The total age and the season of spawning (or: the start of shell growth) were determined by extrapolating the $\delta^{18}O$-based age models and by using the relationship between $\delta^{18}O$ profiles and trace element records and growth increments observed in the shell.

3.7 Strontium isotope analysis

Samples (on average 26 mg) for strontium isotope analysis were obtained by drilling the well-preserved foliated calcite in all shells using a Dremel 3000 dental drill with a 0.5 mm tungsten carbide drill bit. Calcite samples placed in Teflon beakers (Savillex LLC, Eden Prairie, MN, USA), dissolved in subboiled

concentrated (14 M) nitric acid (HNO_3) at 120°C and left to dry out at 90°C overnight, after which the residue was redissolved in 2 M HNO_3. Carbonate-bound strontium in the samples was purified following the ion-exchange resin chromatography method detailed in Snoeck et al. (2015). The $^{87}Sr/^{86}Sr$ of purified Sr samples were determined using a Nu Plasma (Nu Instruments Ltd, Wrexham, UK) multi-collector (MC) ICP-MS unit in operation at the Université Libre de Bruxelles (ULB). During the measurement run, repeated analyses of NIST SRM987 standard solution yielded a ratio of 0.710250 ± 0.000040 (2 SD; N = 14), statistically consistent with the literature value of 0.710248 ± 0.000058 (2 s.e.; McArthur et al., 2001; Weis et al., 2006). All results were corrected for instrumental mass discrimination by internal normalization and normalized to the literature value of NIST SRM987 (0.710248) through a standard-sample bracketing method. For each sample, $^{87}Sr/^{86}Sr$ are reported with 2σ uncertainty (**S8**).

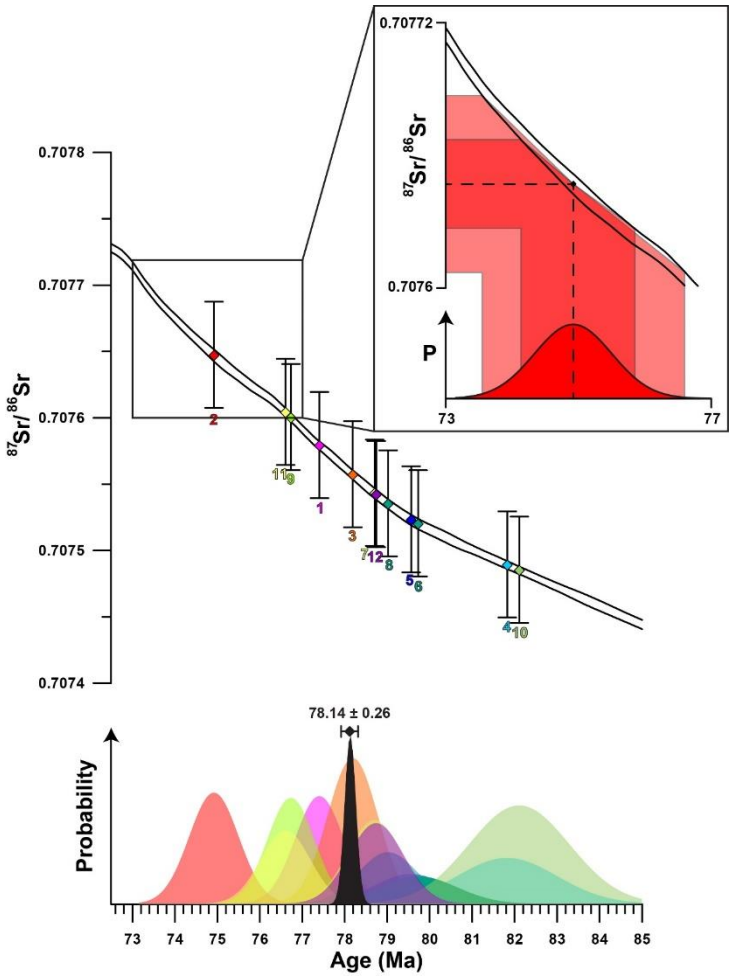

Figure 4: Plot showing the results of Sr-isotopic analyses with error bars (2σ) plotted on the Sr-isotope curve of McArthur et al. (2016; top of image). Numbers below the error bars indicate specimen number. Measurements from the 12 specimens of *R. diluvianum* are represented by parallelograms in different colors which match the probability distributions plotted below. The probability distribution curves in the lower pane show the distribution of uncertainty on each Sr-isotope measurement as well as the uncertainty on the Sr-isotope curve propagated to the age domain (colors of individual shells are the same as in **Fig. 2**). Insert shows schematically how uncertainties of the isotope measurements as well as the isotope curve are propagated into the age domain. The black curve shows the total uncertainty distribution function compiled from the 12 individual measurements following Barlow (2004), with the combined age estimate including uncertainty (2σ) shown above.

3.8 Strontium isotope dating

R. diluvianum specimens were independently dated by comparing $^{87}Sr/^{86}Sr$ values measured in the samples with the Sr-isotope curve in the 2016 Geological Timescale (McArthur et al., 2016). Uncertainties in $^{87}Sr/^{86}Sr$ measurements were propagated into dates by finding the closest date of the mean $^{87}Sr/^{86}Sr$ value as well as the dates of the minimum (-2σ) and maximum (+2σ) $^{87}Sr/^{86}Sr$ values by linearly interpolating ages in the $^{87}Sr/^{86}Sr$ curve matching the measured $^{87}Sr/^{86}Sr$ value, including the uncertainty estimated on the Sr-isotope curve itself. A composite age for the Ivö Klack deposits was obtained by combining the age uncertainty distributions of the individually dated $^{87}Sr/^{86}Sr$ samples into a single age. Due to the non-linear shape of the $^{87}Sr/^{86}Sr$ curve, uncertainties on the $^{87}Sr/^{86}Sr$ ages were asymmetrical. Since no mathematical solution exists for the combination of asymmetric uncertainties, the asymmetric uncertainty on the total age had to be approximated through maximum likelihood estimation using the combined log likelihood function (Barlow, 2003). The approximation of the total uncertainty of combined $^{87}Sr/^{86}Sr$ dating results in this study was carried out using the mathematical approach of Barlow (2004) in R (R Core Team, 2013; Roger Barlow, personal communication; code available on https://zenodo.org/record/1494909). The uncertainty interval of the composite age is represented by 2 times the standard error (~95.5% confidence level). A plot of the uncertainty distributions of the individual specimens and the total uncertainty distribution is shown in **Fig. 4**. Raw $^{87}Sr/^{86}Sr$ data are provided in **S8**.

4. Results

4.1 Strontium isotope dating

Results of strontium isotope analyses are given in **S8**. The mean strontium isotope ratio of all *R. diluvianum* specimens is 0.707552 (±0.000112; 95% confidence level). The compilation of $^{87}Sr/^{86}Sr$ results from 12 specimens of *R. diluvianum* (**Fig. 4**) shows how age estimates from individual specimens have considerable uncertainties (standard deviations around 1 Myr, see **S8**), yet the uncertainty on the composite age is significantly smaller. The composite age for the Ivö Klack deposits is 78.14 Ma (±0.26; 95% confidence

level). This result places the age of the Ivö Klack deposits close to the early/late Campanian boundary when applying a twofold division of the Campanian and in the middle Campanian when applying a threefold division scheme (Ogg et al., 2016). This age estimate is similar to the age obtained when plotting the *B. mammilatus* zone on the recent integration schemes of the Campanian (Wendler, 2013). Earlier estimates (Christensen, 1997; Surlyk and Sørensen, 2010; Sørensen et al., 2015) yielded ages about 2-4 Myr older (80-82 Ma), but those relied on presently outdated and partly incorrect age models.

4.2 Shell structure and preservation

A combination of high-resolution color scans, SEM images and µXRF mapping of shell cross sections reveals that *R. diluvianum* shells consist of thin layers of dark, foliated calcite, interwoven with lighter, more porous carbonate layers (**Fig. 3a-e**). The latter are characterized by higher concentrations of Mn, Fe and Si and lower Sr concentrations (**Fig. 3f-h**). Foliated calcite layers are more densely packed on the inside of the shell, especially in the region of the adductor muscle scar, and at the shell hinge (**Fig. 3a**). They are characterized by high Sr concentrations and low concentrations of Mn, Fe and Si (**Fig. 3f-h**; **S2**). Further away from the shell hinge and the inside of the valve, porous carbonate layers become more dominant. In these regions, µXRF mapping also clearly shows that detrital material (high in Si and Fe) is often found between the shell layers (**Fig. 3f**). SEM images show that the shell structure of *R. diluvianum* strongly resembles that of modern oyster species, as described in previous studies (**Fig. 3b-e**; Carriker et al., 1979; Surge et al., 2001; Ullmann et al., 2010; 2013; Zimmt et al., 2018). The major part of the shell consists of calcite, of which the foliated structures were sampled for chemical analyses in this study. As in modern oyster species, aragonite may originally have been deposited on the resilium of the shell, but this region is not considered for analyses (see outer tip of shell hinge in **Fig. 3a**; Stenzel, 1963; Carriker et al., 1979; Sørensen et al., 2012). Close similarities with modern oysters allow to infer that shell growth in *R. diluvianum* occurred in a similar way as it does in modern oyster species like *Ostrea edulis*, *Crassostrea virginica* and *C. gigas*. From this extrapolation we could estimate the total shell height from microstructural growth markers (dashed lines in **Fig. 3a**; following Zimmt et al., 2018), linking growth to changes in shell chemistry.

4.3 Trace element analyses results

400 The similarity in growth between *R. diluvianum* and modern oyster species is used to assess whether trace
401 element variability in *R. diluvianum* can be interpreted in terms of environmental changes in a similar way
402 as in modern oyster shells (e.g. Surge and Lohmann, 2008; Ullmann et al., 2013; Mouchi et al., 2013;
403 Dellinger et al., 2018). The combination of µXRF and LA-ICP-MS analyses on *R. diluvianum* shells resulted
404 in records of changes in Mg/Ca, Sr/Ca (µXRF), Mg/Li and Sr/Li (LA-ICP-MS) as well as individual
405 concentrations of trace elements such as Mg, Mn, Fe and Sr (**Figure 5**). All chemical analyses were carried
406 out on the dense foliated calcite exposed in cross sections close to the inner edge of the shell valve (**Fig.**
407 **3a**). High-resolution color scans and detailed recording of sampling positions allowed these records to be
408 plotted on a common axis (see **S6**, **S10**). In **Fig. 5**, results of chemical analyses of *R. diluvianum* specimens
409 (including diagenetic parts) are compared with data from three other mollusk taxa (the belemnite
410 *Belemnellocamax mammillatus*, the oyster *Acutostrea incurva* and the radiolithid rudist *Biradiolites*
411 *suecicus*) from Ivö Klack (Sørensen et al., 2015), as well as data from extant oysters (Rucker and Valentine,
412 1961; Surge et al., 2001; Ullmann et al., 2013). Multi-proxy analysis revealed periodic variations in stable
413 isotope and trace element ratios (see **Fig. 6**). The amplitudes of these variations plotted in **Fig. 5** show that
414 Mg and Sr concentrations measured in all three fossil bivalve taxa are similar, while concentrations in the
415 belemnite rostra are much higher. Finally, plots in **Fig. 5b** and **Fig. 5d** demonstrate that diagenetic alteration
416 (evident from elevated Mn concentrations) reduces the Sr concentration in carbonate of all four taxa. Stable
417 oxygen isotope ratios of the shells are affected to a lesser degree (see below). The majority of
418 measurements in all four taxa show very little signs of diagenetic alteration, with most measurements
419 characterized by low (< 100 µg/g) Mn concentrations (**Fig. 5**).
420

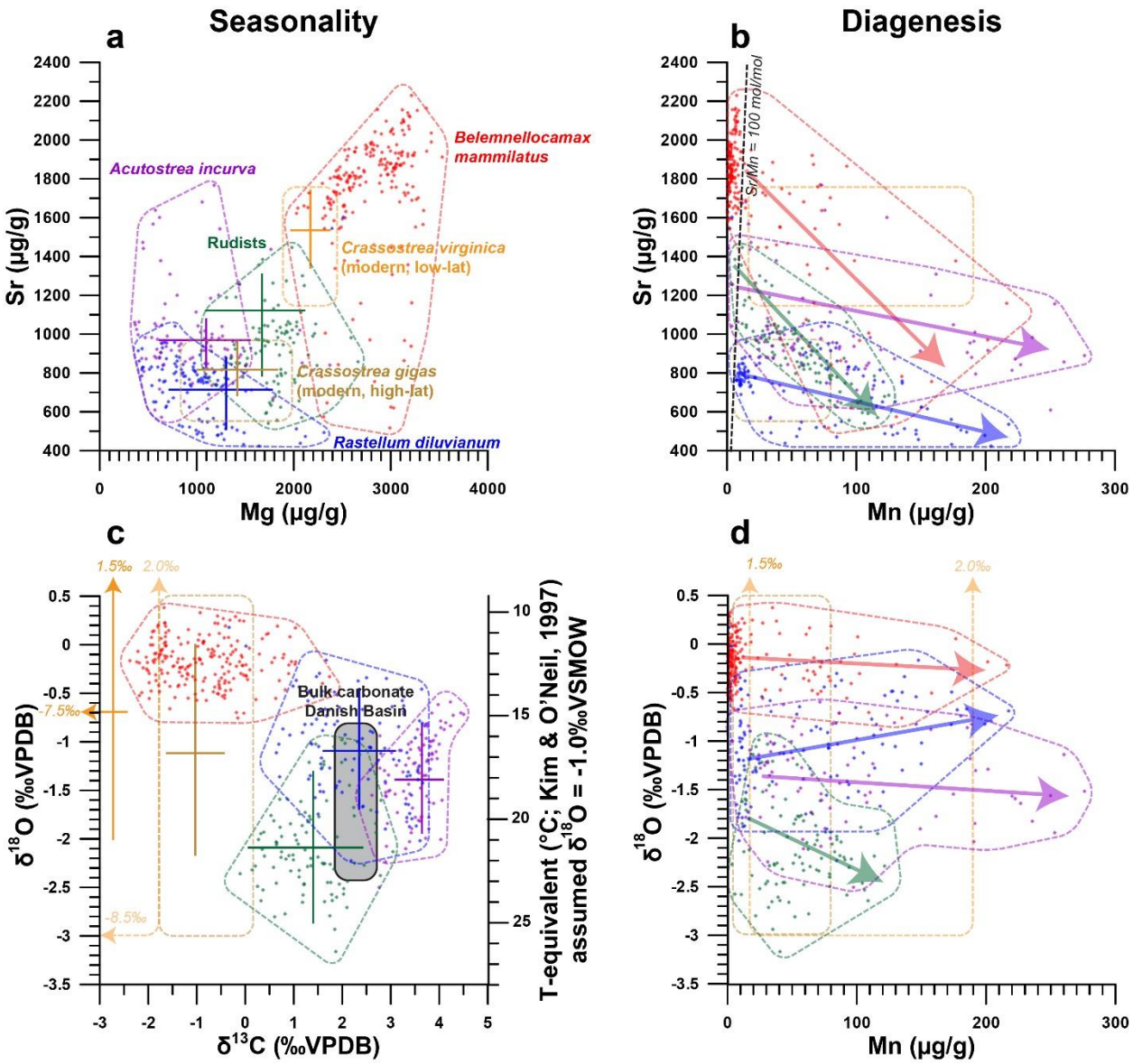

Figure 5: Cross plots summarizing the results of trace element and stable isotope analyses of the oysters *R. diluvianum* (blue), *A. incurva* (purple), the rudist *Biradiolites suecicus* (green) and the belemnite *B. mammilatus* (red, after Sørensen et al., 2015) from the Kristianstad basin. Results from modern *C. gigas* (brown; Ullmann et al., 2013) and *C. virginica* (yellow; Rucker and Valentine, 1961; Surge et al., 2001) oysters are plotted for comparison. Points indicate individual data points, drawn polygons illustrate the range of the data and crosses indicate the extent of seasonality (if present). (**a**) Strontium concentrations plotted against magnesium concentrations. (**b**) Strontium concentrations plotted against manganese concentrations. Arrows indicate the interpreted direction of diagenetic alteration and the black dashed line shows the Sr/Mn diagenesis threshold proposed for belemnite rostra by Sørensen et al. (2015; 100 mol/mol). (**c**) $\delta^{18}O$ plotted against $\delta^{13}C$. Grey area indicates the range of stable isotope ratios measured in Campanian chalk deposits from the nearby Danish Basin by Thibault et al. (2016) (**d**) $\delta^{18}O$ plotted against manganese concentrations, with arrows indicating proposed direction of diagenetic alteration.

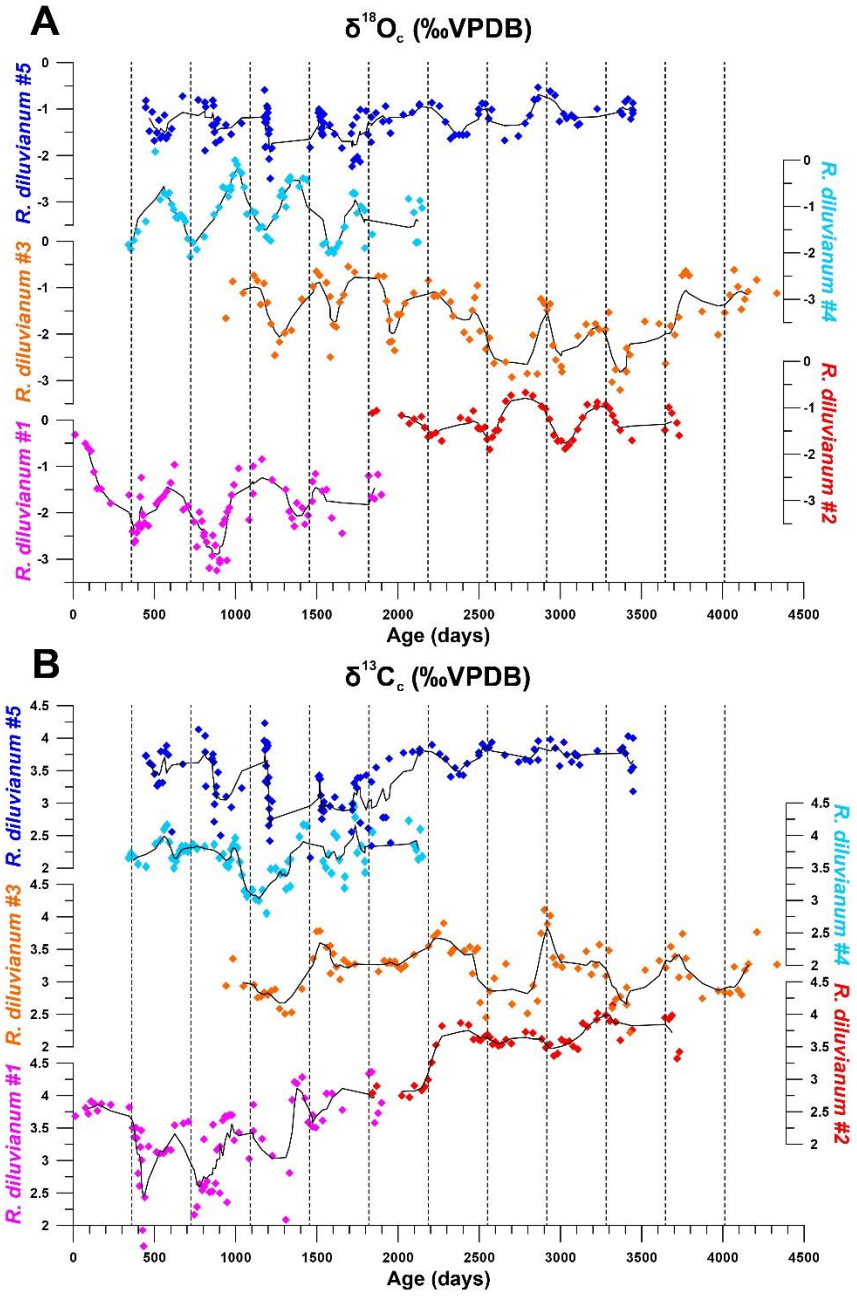

433

434 ***Figure 6****:* Overview of stable oxygen (**A**) and carbon (**B**) profiles from all five shells in which stable isotope profiles are measured
435 plotted against ontogenetic ages. Black lines indicate 5point running averages through the time series. Vertical dashed lines separate
436 years of growth. All vertical axes of $\delta^{18}O$ and $\delta^{13}C$ have the same scale. Colors coding is the same as in **Figure 7**.

437

4.4 Stable isotope records

An overview of stable isotope results of *R. diluvianum* (IRMS, only for shells 1-5, see **Fig. 2**) compared with the different taxa in Kristianstad Basin and modern oyster data is given in **Figure 5**. Stable isotope ratios of the rudist and oyster shells overlap, while belemnite rostra of the species *B. mammillatus* are characterized by much lower $\delta^{13}C$ and heavier $\delta^{18}O$ values. This suggests that $\delta^{13}C$ in belemnite rostra from this species are affected by vital effects while heavier $\delta^{18}O$ values of the belemnites suggest that belemnites lived most of their life away from the coastal environment (in deeper waters), as previously suggested by Sørensen et al. (2015). In contrast, stable isotope ratios recorded in the bivalve shells overlap and match the isotope ratios measured in Campanian chalk deposited in the neighboring Danish Basin (Thibault et al., 2016). Records of $\delta^{13}C$ and $\delta^{18}O$ in the growth direction through *R. diluvianum* shells exhibit periodic variations (**Figure 6**). These variations are much more regular in $\delta^{18}O$ records, which show extreme values below -3‰ and up to 0‰ VPDB (**Fig. 6a**). Some shells, such as *R. diluvianum* 3 (**Fig. 7**), exhibit longer term trends on which these periodic variations are superimposed. These trends suggest the presence of multi-annual cyclicity with a period in the order of 10-20 years, but the length of *R. diluvianum* records (max. 10 years) is smaller than the estimated period of these changes and is therefore insufficient to statistically validate the presence of this cyclicity.

The extreme values in $\delta^{18}O$ records translate to tentative temperatures in the range of extremes of 12°C to 26°C when assuming a constant $\delta^{18}O_{sw}$ value of -1.0‰ (e.g. Thibault et al., 2016) and applying the temperature relationship of Kim and O'Neil (1997). However, the assumption of constant $\delta^{18}O_{sw}$ may add bias to the temperature reconstructions, as seawater composition may not have been constant or reflect the marine value year-round in the nearshore Ivö Klack setting. Carbon isotope ratios ($\delta^{13}C$) do not always follow the same trends as $\delta^{18}O$ records (**Fig. 6b**). In many parts of *R. diluvianum* shells, there is a clear covariation between the two isotope ratios, suggesting $\delta^{13}C$ is affected by seasonal changes. However, in other parts this correlation is less clear, suggesting that other (non-seasonal) factors play a role in determining the $\delta^{13}C$ of shell material.

4.5 Age models

Modelling the growth of *R. diluvianum* bivalves from seasonal variations in $\delta^{18}O$ profiles yielded age models, growth rate estimates and reconstructions of water temperature variations during the lifetime of the bivalves. Due to the clear seasonal patterns in $\delta^{18}O$ records (**Fig. 6a**, **Fig. 7**), modelled $\delta^{18}O$ profiles closely approximated the measured $\delta^{18}O$ profiles (total $R^2 = 0.86$, N = 412, see **S5** and **S9**), lending high confidence to shell age models (see example in **Fig. 7**). Modelling allowed all proxies measured in the shells of *R. diluvianum* to be plotted against shell age, clearly revealing the influence of seasonal variations in environmental parameters on shell chemistry (**S10**). The age models reveal clear, statistically significant ($p < 0.05$) ontogenetic trends in Mg/Li, Sr/Li and $\delta^{13}C$ in nearly all specimens of *R. diluvianum* (see **Table 1**). In 3 out of 5 shells, $\delta^{13}C$ increases with age (see **Fig. 6b** and **Table 1**) with ontogenetically older specimens (e.g. *R. diluvianum* #2) yielding overall higher $\delta^{13}C$ values (**Fig. 6b**). The distribution of slopes of ontogenetic trends in Li/Ca cannot be distinguished from random variation. Therefore, no predictable ontogenetic trends were found for Li-proxies in *R. diluvianum* shells.

	Li/Ca			$\delta^{13}C$		
	slope (mol/(mol*yr))	R2	p-value	slope (‰/yr)	R2	p-value
***R. diluvianum* 1**	-1.29E-06	0.053	4.32E-08	0.346	0.426	8.86E-07
***R. diluvianum* 2**	3.74E-07	0.101	2.68E-05	0.169	0.440	8.19E-08
***R. diluvianum* 3**	3.86E-07	0.004	5.32E-03	-0.004	0.001	8.09E-01
***R. diluvianum* 4**	-1.07E-06	0.025	8.78E-04	0.023	0.009	3.99E-01
***R. diluvianum* 5**	-1.94E-06	0.030	6.30E-14	0.136	0.492	5.53E-11
***R. diluvianum* 6**	-2.32E-06	0.117	8.75E-15			
***R. diluvianum* 7**	-7.49E-07	0.029	4.77E-02			
***R. diluvianum* 8**	-1.19E-07	0.003	2.90E-01			
***R. diluvianum* 9**	-4.63E-07	0.010	5.65E-02			
***R. diluvianum* 10**	1.59E-06	0.015	1.61E-02			
***R. diluvianum* 11**	-1.87E-06	0.199	4.25E-12			
***R. diluvianum* 12**	-4.55E-07	0.003	4.19E-01			
	$p(\chi^2)$		0.976	$p(\chi^2)$		1.000
	$p(\chi^2)$ weighed by R2		0.976	$p(\chi^2)$ weighed by R2		1.000
	$p(\chi^2)$ weighed by p-value		0.961	$p(\chi^2)$ weighed by p-value		0.998

Table 1: *Overview of the slopes of ontogenetic trends in Li/Ca and $\delta^{13}C$ records. P-values on the bottom of the table show that the distribution of Li/Ca slopes is statistically indistinguishable from random.*

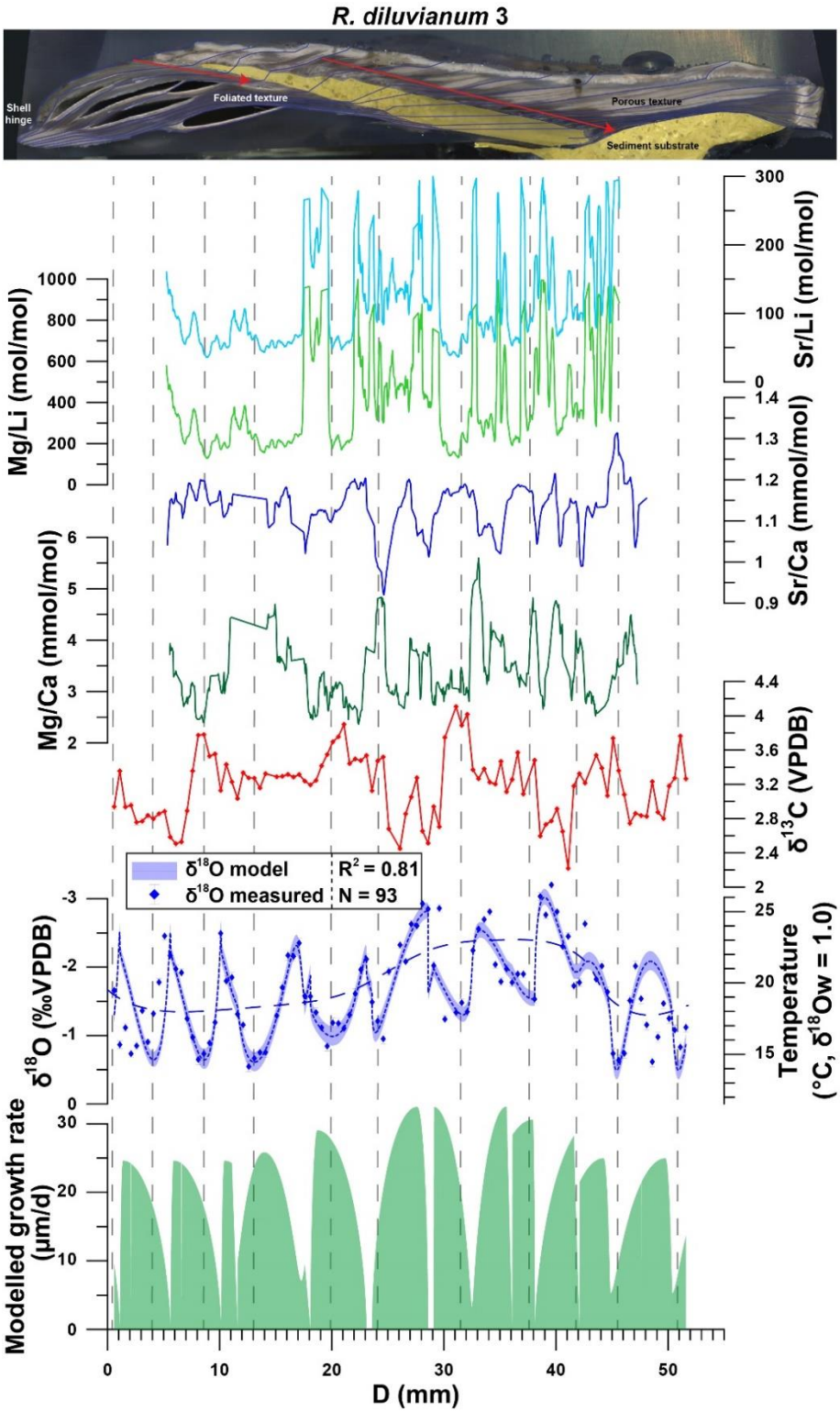

Figure 7: Example of multi-proxy records measured in *R. diluvianum* specimen 3 plotted against distance in growth direction (see image on top and **Fig. 3** for reference). From top to bottom, records of Sr/Li (light blue), Mg/Li (light green), Sr/Ca (dark blue), Mg/Ca (dark green), $\delta^{13}C$ (red), $\delta^{18}O$ (blue dots with error bars) and modelled growth rate (light green fill) are plotted. The shaded blue curve plotted underneath the $\delta^{18}O$ record illustrates the result of growth and $\delta^{18}O$ modelling and its propagated error (vertical thickness of curve, 2SD). The dashed blue curve plotted on top of the $\delta^{18}O$ record shows the observed multi-annual trend in the data. Vertical dashed lines separate growth years. Multi-proxy plots for all specimens are given in **S10**.

481

5. Discussion

5.1 Preservation

The relative lack of burial and tectonic activity in the Kristianstad Basin has provided ideal circumstances for the nearly immaculate preservation of *R. diluvianum* shells in the Ivö Klack locality (Kominz et al., 2008; Surlyk and Sørensen, 2010). The excellent state of these shells is evident by the preservation of original (porous and foliated) microstructures that closely resemble those reported for several species of modern ostreid shells (Carriker et al., 1979; Surge et al., 2001; Ullmann et al., 2010; 2013; Zimmt et al., 2018; **Fig. 2-3**). High magnification SEM images demonstrate the excellent preservation of foliated and vesicular calcite structures in *R. diluvianum* shells (**Fig. 3b-d**). The preservation state of *R. diluvianum* shells meets the SEM-based preservation criteria for robust stable isotope analysis set by Cochran et al. (2010). MicroXRF mapping reveals that the foliated calcite in the shells is characterized by high Sr concentrations and low concentrations of Mn, Fe and Si, elements which are generally associated with diagenetic alteration (e.g. Brand and Veizer, 1980; Al-Aasm and Veizer, 1986a; Immenhauser et al., 2005; **Fig. 3b-h**). Trends in bulk Mn and Sr concentrations observed in all fossil species from Ivö Klack (**Fig. 5b;** including less well-preserved parts) likely point towards a diagenetic process affecting a less well-preserved subset of the data. The lack of covariation between Mn concentration and $\delta^{18}O$ shows that there is little evidence for meteoric diagenesis in these shells (**Fig. 5d**; Ullmann and Korte, 2015). Instead, these patterns are best explained by early marine cementation of porous carbonate structures from sea water with similar temperature and $\delta^{18}O$ as the living environment (see also Sørensen et al., 2015).

Typically, a Mn concentration threshold of 100 µg/g is applied below which Cretaceous low-magnesium carbonates are assumed suitable for chemical analysis (Steuber et al., 2005; Huck et al., 2011). Strontium concentrations above 1000 µg/g have also been used as markers for good preservation, since diagenetic processes can cause strontium to leach out of carbonates (e.g. Brand and Veizer, 1980; Huck et al., 2011; Ullmann and Korte, 2015). Previous studies of belemnites in Kristianstad Basin proposed a molar Sr/Mn threshold of 100 for belemnite rostra (Sørensen et al., 2015). However, the height of thresholds used for diagenetic screening differs widely in the literature due to variety between species, fossil matrices and burial histories (e.g. Veizer, 1983; Steuber et al., 1999; Ullmann and Korte, 2015; de Winter and Claeys, 2016).

Applying these thresholds risks introducing biases to chemical datasets from fossil shells and may not be an ideal method for diagenetic screening. Furthermore, large variation in the *in vivo* incorporation of Mn and Sr in mollusk shell carbonate and a strong dependence on the diagenetic setting can make the interpretation of shell preservation from trace element ratios alone highly ambiguous (Ullmann and Korte, 2015). The complex patterns in multi-proxy datasets in this study (**Fig. 5**) merit great care in applying simple, general thresholds for grouping different processes of carbonate diagenesis. Therefore, in this study, a multi-proxy approach is applied for diagenetic screening in which data is excluded based on a combination of Si, Ca, Mn, Fe and Sr concentrations, $\delta^{18}O$ values as well as SEM and visual observations of the shell structure at the location of measurement.

5.2 Dating the Ivö Klack locality

While previous attempts at dating Campanian strata mainly focused on relative dating using magneto- and biostratigraphy (Montgomery et al., 1998; Jarvis et al., 2002; Voigt et al., 2010), integration of cyclostratigraphic approaches in this integrated stratigraphic framework has recently allowed to constrain the age of the Campanian deposits more precisely (Voigt and Schönfield, 2010; Thibault et al., 2012; Wendler, 2013; Thibault et al. 2016). Unfortunately, these rarely cover the time interval in which the Ivö Klack sediments were deposited (e.g. Wendler, 2013; Perdiou et al., 2016). Strontium isotope dating places the Ivö Klack deposits at 78.14 ± 0.26 Ma (**Fig. 4**). When plotting the obtained age of 78.14 Ma on the compilation by Wendler (2013), the age of the Ivö Klack falls slightly above the early/late Campanian subdivision (which is placed at ~78.5 Ma), while the *B. mammilatus* biozone is defined as late early Campanian. Influx of radiogenic strontium-rich weathering products from the nearby Transscandinavian Igneous Belt may bias age estimates from strontium isotope ratios (Högdahl et al., 2004). However, studies of modern strontium isotope ratio variability (Palmer and Edmond, 1989) and the potential bias of strontium isotope ratios in shallow-water carbonates (Kuznetsov et al., 2012; El Meknassi et al., 2018) show that the effect of such inputs on strontium isotope dating results is generally negligible, except in semi-confined shallow-marine basins characterized by considerable freshwater input and low salinities (<7 psu). No evidence exists for such exceptional conditions at Ivö Klack (see **2.1**). We therefore conclude that our strontium isotope age estimate, together with biostratigraphic constraints, places the Ivö Klack locality in the earliest late Campanian. The refined dating of the Ivö Klack deposits and fossils allows the results of

sclerochronological investigations presented in this work to be placed in the context of longer-term climate reconstructions with improved precision.

5.3 Trace element variability

Extracted ranges in seasonal scale periodic variability in Mg/Ca, Sr/Ca, Mg/Li and Sr/Li in all 12 *R. diluvianum* shells (**Fig. 8**) show that it is not straightforward to interpret these records in terms of temperature changes. Some of this difficulty arises from the large inter-shell variability in trace element ranges, mostly expressed in strong positive correlations between Sr/Li and Mg/Ca ($R^2 = 0.76$) and between Sr/Li and Mg/Li ($R^2 = 0.93$). The benthic foraminifera proxy transfer function for Mg/Li (Bryan and Marchitto, 2008) does not work for *R. diluvianum* (temperatures >50°C), presumably due to typically lower Mg concentrations in foraminifera compared to bivalves (Yoshimura et al., 2011). Bivalve-specific temperature relationships of Mg/Ca (Surge and Lohmann, 2008; based on *Crassostrea virginica*), Sr/Li (Füllenbach et al., 2015; based on *Cerastoderma edule*) and Mg/Li (Dellinger et al., 2018; based on *Mytilus edulis*) yield temperatures in the same range as those reconstructed from stable oxygen isotope measurements (10-20°C). However, Sr/Li-based temperature trends are opposite to those based on Mg-proxies, suggesting that they cannot both be applicable to *R. diluvianum*. Poorly constrained changes in seawater chemistry (Mg/Ca and Sr/Ca ratios of ocean water) also hinder these trace element-based reconstructions (Lear et al., 2003; Coggron et al., 2010; Rausch et al., 2013). The strong Mg/Li-Sr/Li correlation indicates that both proxies are likely strongly affected by the specimen-specific ontogenetic trends in Li/Ca described in **Table 1**. This, together with the large inter-specimen variability shows that both Li-proxies cannot be used as temperature proxies in *R. diluvianum*. An annual stack of all proxies shows that the positive correlation between Mg/Ca and $\delta^{18}O$ (**Fig. 9**) is opposite to the temperature-relationships found in modern oyster species (Surge and Lohmann, 2008; Mouchi et al., 2013; Ullmann et al., 2013). This together with the reduced seasonal variability (1.2 mmol/mol versus 4-10 mmol/mol in modern oysters; Surge and Lohmann, 2008; Mouchi et al., 2013) and the large (>3 mmol/mol; **Fig. 8**) inter-specimen variability both in mean value and seasonal Mg/Ca range rules out Mg/Ca as a reliable temperature proxy in *R. diluvianum*. This result demonstrates that earlier successful attempts to establish calibration curves for Li- and Mg-based temperature proxies (e.g. Füllenbach et al., 2015; Dellinger et al., 2018) are probably strictly limited to these bivalve species or close relatives. The same conclusion was also drawn by Dellinger et al. (2018) based

on Li/Mg and Li isotope ratio measurements in biogenic carbonates. The lack of Mg/Li or Sr/Li calibrations in modern oyster shells limits the interpretation of the results of this stud. Establishing such calibrations using modern oysters in cultured experiments may allow these proxies to be used for reconstructions from fossil oyster shells in the future.

While not a likely candidate for reconstructing temperature (Gillikin et al., 2005; Schöne et al., 2013; Ullmann et al., 2013), seasonal Sr/Ca fluctuations and relationships between Sr/Ca and $\delta^{18}O$ are consistent between individuals (**Fig. 8-9**; see also **S6**). This allows Sr/Ca ratios to be used together with microstructural observations of growth increments as basis for seasonal-scale age models in shells for which no $\delta^{18}O$ measurements were done. Both mean Sr/Ca values and seasonal variability in *R. diluvianum* are consistent with those observed in the same microstructure in modern *Crassostrea gigas* growing in a similar environment (0.8-1.0 mmol/mol; Ullmann et al., 2013), suggesting a consistent incorporation of Sr by different oyster taxa over time. It must be noted that one should be cautious when directly comparing trace element concentrations in biogenic calcite between different time periods, as the seawater composition of Late Cretaceous oceans (e.g. concentrations of Mg, Ca, Sr and especially Li) may have been different from that of the present-day ocean (Stanley and Hardie, 1998; Coggon et al., 2010; Rausch et al., 2013). Local enrichments in seawater Sr concentrations at Ivö Klack driving increased Sr composition in *R. diluvianum* are unlikely, since Sr/Ca ratios exhibit only small (2-3%) lateral variability in the world's oceans (De Villiers, 1999). Because Sr/Ca ratios in Late Cretaceous oceans were twice as low as in the modern ocean, one would expect, for example, that Sr concentrations in Late Cretaceous biogenic carbonate would be twice as low as those in carbonates formed in the modern ocean, if the partition coefficient between seawater concentrations and shell concentrations remains constant (Stanley and Hardie, 1998; de Winter et al., 2017a). The fact that this reduction in Sr concentrations relative to the modern ocean is not observed in *R. diluvianum* may entail that there is a fixed physiological limit to oyster's discrimination against building Sr into their shells that is independent of ambient Sr concentrations.

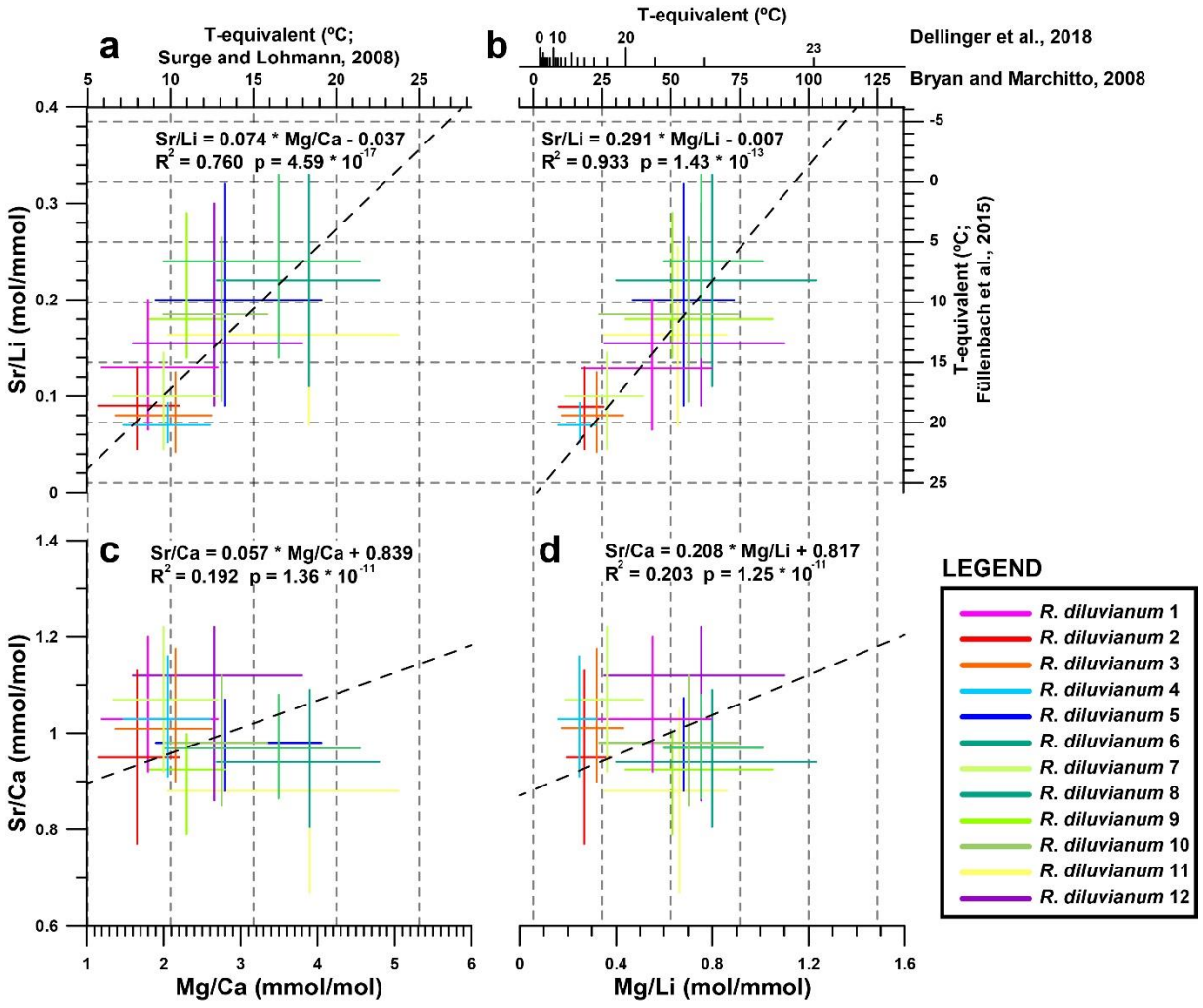

Figure 8: Cross plots showing the extent of interpreted seasonality observed in records of four trace element proxies in all 12 *R. diluvianum* specimens. Colors of lines of individual shells correspond to colors indicated in **Fig. 2**. Temperature conversions from previously published regressions of the proxies with temperature are shown on opposite axes with grey dashed lines corresponding to major tick marks on the temperature scale (**a**) Sr/Li plotted against Mg/Ca showing a strong significant intra-shell correlation. (**b**) Sr/Li plotted against Mg/Li showing a strong significant intra-shell correlation due to dominant variations in Li concentration. Note that two different Mg/Li temperature calibrations were explored. (**c**) Sr/Ca plotted against Mg/Ca showing weak but significant intra-shell correlation. (**d**) Sr/Ca plotted against Mg/Li showing a weakly significant intra-shell correlation. Data for this plot is found in **S13**.

600

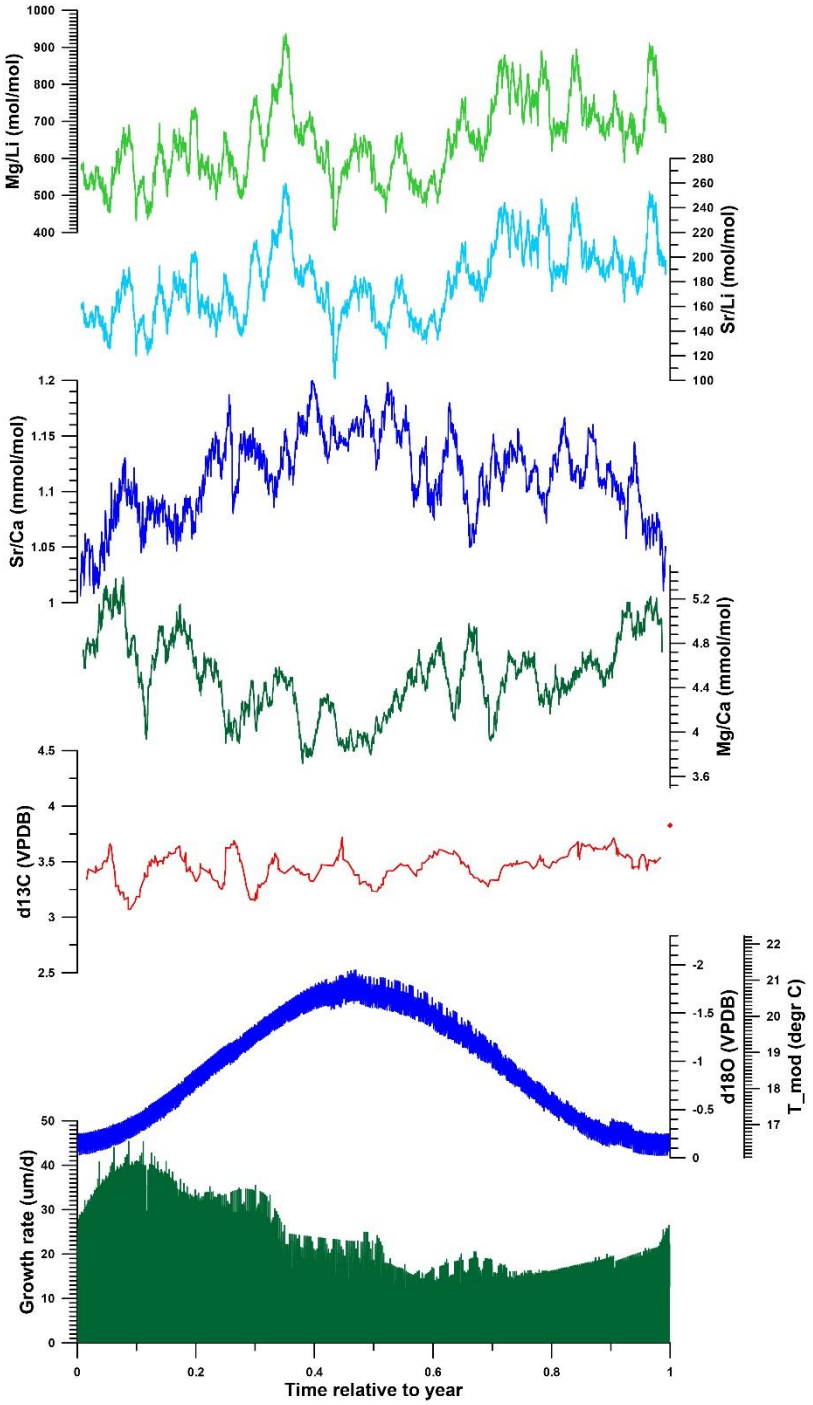

Figure 9: Composite of multi-proxy records from all *R. diluvianum* shells stacked and plotted on a common time axis of 1 year to illustrate the general phase relationships between various proxies in the shells. Records were colored as in **Fig. 7**. Annual stacks plotted in this figure were produced by applying age models on all multi-proxy records, plotting all results against their position relative to the annual cycle and applying 20 point moving averages.

601

5.4 Temperature seasonality

An annual stack of all *R. diluvianum* proxy records shows a $\delta^{18}O_c$-based temperature variability in Ivö Klack of 16-21°C when assuming a constant $\delta^{18}O_{sw}$ of -1‰VSMOW. However, comparison with $\delta^{18}O$-seasonality in individual specimens shows that the annual stack severely dampens seasonality due to small phase shifts in maximum and minimum temperatures, small uncertainties in the age models between years and specimens, and inter-annual differences and longer-term trends in temperature (see **Fig. 6**). A more accurate estimate of the seasonal extent is obtained by calculating the seasonal range from the coolest winter temperatures (12.6°C in *R. diluvianum* 4; **Fig. 6**; **S10**) with the warmest recorded summer temperature (26°C in *R. diluvianum* 1; **Fig. 6**; **S10** which yields an extreme maximum seasonal sea surface temperature (SST) range of ±13.4°C.

A complication of these reconstructions is the assumption of constant $\delta^{18}O_{sw}$ of -1‰VSMOW, which is unlikely to be completely accurate in the nearshore Ivö Klack locality. Comparison with data from *Crassostrea gigas* growing in a similar nearshore environment (Ullmann et al., 2010; German North Sea coast, 54°N) show that such an environment away from large river mouths can typically experience seasonal salinity fluctuations of ~4 psu resulting in a dampening of the seasonal $\delta^{18}O_c$ cycle by ~0.5‰VPDB. Such a salinity-effect would reduce our reconstructed 13-26°C seasonal temperature range by ~2°C to 14-25°C.

In addition, mean annual $\delta^{18}O_{sw}$ values can be considerably lighter than the global average seawater composition (e.g. -1‰ to -1.5‰VSMOW compared to global ocean mean of 0‰VSMOW in Ullmann et al., 2010). Considering such a deviation would reduce reconstructed temperatures by 4-6°C to 10-21°C, much colder than open marine reconstructions of the Boreal Chalk Sea by Thibault et al. (2016). This result would be in strong disagreement with a recent study by Tagliavento et al. (2019) in which clumped isotope analyses (which does not rely on the assumption of constant $\delta^{18}O_{sw}$) were used to correct the $\delta^{18}O_c$-based reconstructions of the Boreal Chalk, and which yielded *higher* temperatures (~26°C MAT for open marine SST) and a correction of $\delta^{18}O_{sw}$ towards 1-1.5‰ heavier values (resulting in a Campanian $\delta^{18}O_{sw}$ of -0.5-0‰VSMOW). Another caveat is that salinity effects on local $\delta^{18}O_{sw}$ strongly depend on the local $\delta^{18}O_{sw}$ of the local freshwater source (riverine or precipitation), which in the present-day higher mid-latitudes is

around -7‰VSMOW to -8‰VSMOW (e.g. Ullmann et al., 2010), but this is impossible to constrain at Ivö Klack during the Campanian within the scope of this study.

If local $\delta^{18}O_{sw}$ values at Ivö Klack were indeed 1-1.5‰ reduced with respect to those in the fully marine Boreal Chalk Sea, and marine $\delta^{18}O_{sw}$ was around 0-0.5‰VSMOW rather than the assumed -1‰VSMOW, the effects of these two biases cancel each other out, and the best estimation of the extreme seasonal SST range at Ivö Klack based on this study's data would be 14-25°C with a MAT of 19°C. This MAT is comparable to the MAT of the late early Campanian Boreal Chalk Sea waters of 17-19°C calculated based on coccolith-$\delta^{18}O_c$ (Lowenstam and Epstein, 1954; Jenkyns et al., 2004; Friedrich et al., 2005; Thibault et al., 2016), and slightly warmer than mean annual air temperatures from this paleolatitude based on phosphate-$\delta^{18}O$ reconstructions paleolatitude (±15°C; Amiot et al., 2004). However, Ivö Klack SST's are ~6°C colder than the clumped isotope-based reconstructions from marine chalk samples (Tagliavento et al., 2019). The latter could indicate that coastal SST's and air temperatures were much colder than marine temperatures in the Campanian higher latitudes, but such temperature differences are highly unusual compared to modern climates. Alternatively, this difference could highlight a severe temperature bias in (both phosphate and carbonate) $\delta^{18}O$-based reconstructions, which should be further investigated using independent proxies such as the clumped isotope paleothermometer (e.g. de Winter et al., 2018; Tagliavento et al., 2019).

Modelled growth rates in *R. diluvianum* peak near the end of the low temperature season and average growth rates are lowest shortly after the temperature maximum (**Fig. 9**). This phase shift between temperature and growth rate could indicate that growth in *R. diluvianum* in this setting was not limited by low temperatures, as observed in modern mid- to high-latitude oysters (Lartaud et al., 2010). High temperature extremes (>25°C) may have slowed or stopped growth, as recorded in modern low latitude settings (Surge et al., 2001). Heat shock has been shown to limit the growth of modern oysters (*Crassostrea gigas*; Li et al., 2007), although the relatively moderate SST seasonality suggests that such very high (>25°C) temperatures were not common at the Ivö Klack locality (**Fig. 6**). In addition, the use of $\delta^{18}O$ records from multiple specimens reduces the effects of growth cessations of individuals on seasonal SST reconstructions and allows the full seasonal range in SST to be resolved.

The reconstructed MAT for Ivö Klack is 7-8 degrees warmer than the present-day mean annual SST in the North and Baltic seas at similar latitude (e.g. 2-18°C monthly seasonality range in Baltic Sea Karlskrona, Sweden, 56°N and 4-18°C monthly seasonality range in North Sea Esbjerg, Denmark, 55°N; IRI/LDEO Climate Data Library, 2020). SST seasonality at Ivö Klack (11°C) is significantly lower than the 14-16°C temperature seasonality that occurs in the present-day Baltic and North seas. Data on temperature seasonality in the Late Cretaceous are scarce, especially in high-latitude settings. However, comparison with data on Cretaceous seasonality between 15°N and 35°N paleolatitude (Steuber et al., 2005) shows that while MAT at 50°N was significantly lower than those at lower latitudes (19°C vs. 25-30°C respectively), the seasonal temperature range during cooler periods in the Late Cretaceous was remarkably similar between latitudes (10-15°C in subtropical latitudes vs. ±14°C in this study). This observation contrasts with the present-day situation in Northern Africa and Europe, in which seasonal temperature ranges are generally much higher in mid- to high-latitudes (30-50°N) than in lower latitudes (10-30°N; Prandle and Lane, 1995; Rayner, 2003; Locarnini et al., 2013; NOAA, 2020). Our SST reconstructions also show that Late Cretaceous latitudinal temperature gradients and mid- to high-latitude seasonality were larger than previously assumed based on climate model results (Barrera and Johnson, 1999; Hay and Floegel, 2012; Upchurch et al., 2015).

5.5 Shell growth and ontogeny

5.5.1. Growth curves

Growth curves of individual *R. diluvianum* specimens clearly converge to a general growth development curve for the species (**Fig. 10**). Considering that these growth curves are based on $\delta^{18}O$ and Sr/Ca transects in different stages of life in different specimens (large age variation; see **Fig. 8**), individual growth curves are remarkably similar. The growth of *R. diluvianum* takes the typical shape of the asymptotic Von Bertalanffy curve, in which shell height (H_t) development with age (t) is related to a theoretical adult size H_{max} and a constant k in the equation: $H_t[mm] = H_{max} * \left(1 - e^{k*(t[yr]-t_0)}\right)$, with t_0 representing the time at which the growth period started (always zero in this case; Von Bertalanffy, 1957). When this formula is regressed over all modelled growth data of all shells (1 data point per day, 15146 points in total), the fit with an H_{max} of ±120.3 mm and a K value of ±0.32 is very good (R^2 = 0.79; see **Fig. 10**).

682 The consistency in growth curves between individuals of *R. diluvianum* is surprising as modern oyster
683 species are known to exhibit large variations in growth rates and shell shapes as a function of their colonial
684 lifestyle, which often limits the growth of their shells in several directions (Galtsoff, 1964; Palmer and
685 Carriker, 1979). The strong resemblance of growth between individuals and the close fit of the idealized
686 Von Bertalanffy growth model suggests that growth of *R. diluvianum* at Ivö Klack was relatively unrestricted
687 in space. This hypothesis is consistent with the apparent mode of life of *R. diluvianum* in Ivö Klack cemented
688 next to each other in loose groups, subject to strong wave action and turbulence, but with little competition
689 for space due to the high-energy environment (Surlyk and Christensen, 1974; Sørensen et al., 2012). The
690 shape of the growth curve of *R. diluvianum* resembles that of modern Chesapeake Bay oysters
691 (*Crassostrea virginica*), which exhibit a slightly larger modelled maximum height (150 mm) and a slightly
692 smaller K-value (0.28). A larger subset of *R. diluvianum* specimens studied by Sørensen et al. (2012)
693 demonstrates that these bivalves could grow up to 160 mm in height. The curvature of the growth of *R.*
694 *diluvianum* (K-value) is also similar to that found for other modern shallow marine bivalve species (e.g.
695 *Macoma balthica*, K = 0.2-0.4; Bachelet, 1980; *Pinna nobilis*, K = 0.33-0.37; Richardson et al., 2004) and
696 significantly higher than in growth curves of deep shelf-dwelling bivalves (e.g. *Placopecten magellanicus*,
697 K = 0.16-0.24; MacDonald and Thompson, 1985; Hart and Chute, 2009) or bivalves from cold habitats (e.g.
698 North Atlantic *Arctica islandica*, K = 0.06; Strahl et al., 2007). This reflects the high growth rates (steeper
699 growth curves, higher K-values) of shallow marine bivalves compared to species living in more unfavorable
700 or restricting (colder or deeper) habitats, with *R. diluvianum* clearly being part of the former group.
701

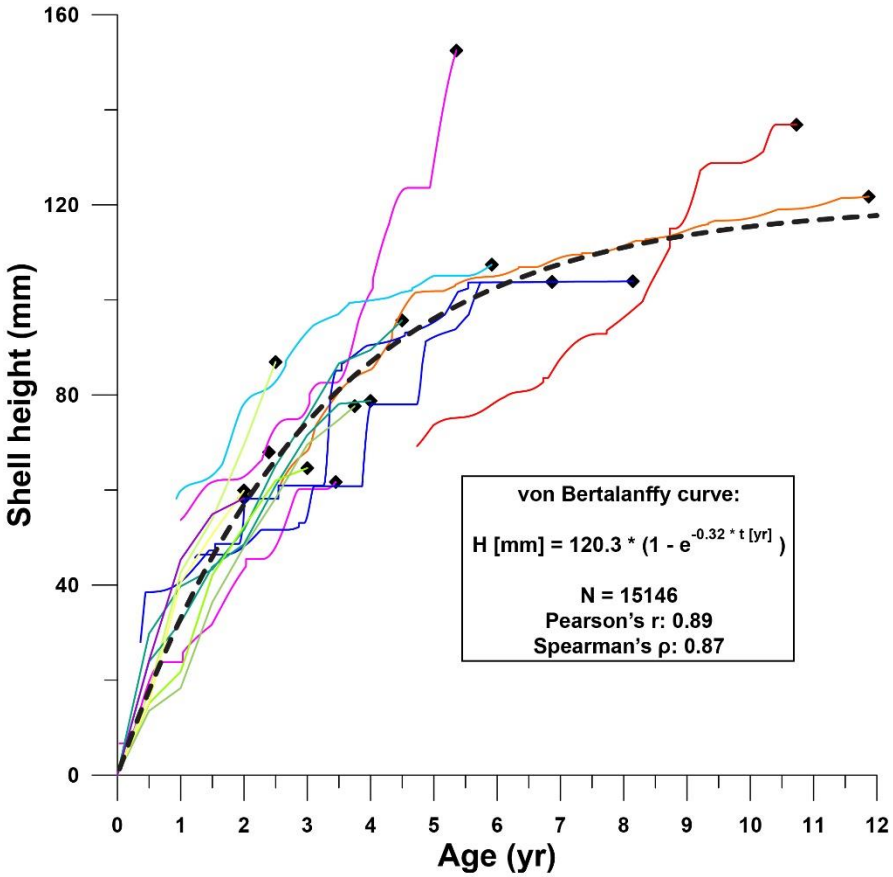

Figure 10: Shell height plotted against age for all *R. diluvianum* records (see **Fig. 8** for color legend of lines representing individuals). The similarity between growth curves of different specimens allows a Von Bertalanffy curve to be fitted to the data with high confidence. Sinusoidal patterns superimposed on all growth curves are caused by seasonal variability in growth rate (see **Fig. 6-7**). Data found in **S9**.

5.5.2 Seasonal growth

To study variability in minimum growth temperature (**Fig. 11a**), length of the growth season and time of year on which maximum growth occurs (**Fig. 11b**), we isolated individual growth years from all age models of the five shells in which $\delta^{18}O$ curves were measured (**Fig. 11**). The onset and end of each growth year correspond to maxima in $\delta^{18}O$ values (minima in temperatures). The onset of the first growth year in each shell at its precise position relative to the seasonal temperature cycle showed in which season spawning occurred (**Fig. 11b**). All data used to create plots in **Fig. 11** are provided in **S14**. Relationships between these growth parameters are summarized in **Table 2**.

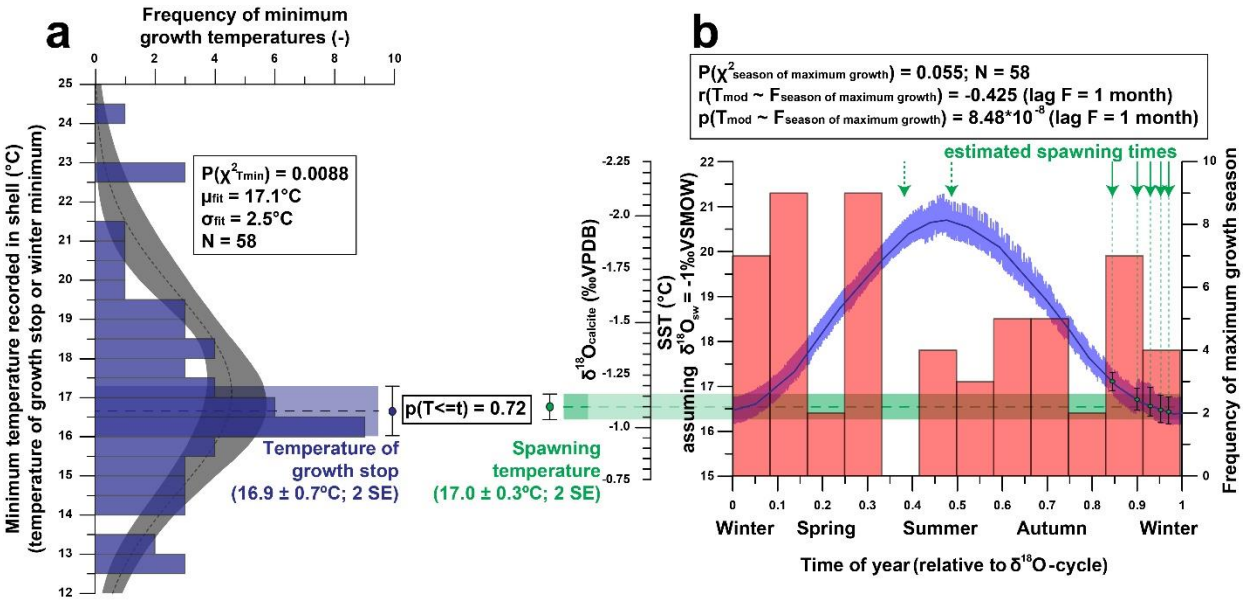

Figure 11: Overview of statistical evaluation of growth parameters of *R. diluvianum* derived from age modelling in shells 1-5. (**a**) Histogram of minimum temperatures of growth (equivalent to the time at which growth stops or the minimum yearly temperature) in *R. diluvianum* showing that the temperature on which growth slows coincides with that of the spawning season (p = 0.717). (**b**) Histogram of the season of maximum growth relative to the $\delta^{18}O$ seasonality cycle shows no significant concentration towards a favorable growing season while moments of first growth (spawning) are significantly concentrated towards the low-$\delta^{18}O$ season.

N = 58	Total annual growth (µm)	Maximum growth rate (µm/d)	Length of season (d)	Minimum growth temperature (°C)	Temperature seasonality (°C)	Average temperature (°C)
Temperature seasonality (°C)	R^2 0.024 p $2.16*10^{-11}$	R^2 0.053 p $6.73*10^{-10}$	R^2 0.403 p $2.15*10^{-22}$			
Average temperature (°C)	R^2 0.020 p $2.29*10^{-11}$	R^2 0.027 p $6.95*10^{-7}$	R^2 0.008 p $2.87*10^{-21}$	R^2 0.565 p $3.44*10^{-7}$		
Age (yr)	R^2 0.000 p $1.11*10^{-9}$	R^2 0.062 p $9.74*10^{-12}$	R^2 0.002 p $1.59*10^{-22}$	R^2 0.002 p $1.05*10^{-30}$	R^2 0.059 p $4.59*10^{-1}$	R^2 0.000 p $1.09*10^{-35}$

Table 2: Overview of statistical evaluation of growth parameters of *R. diluvianum* derived from age modelling in shells 1-5. Coefficients of determination (R^2) and p-values were determined for relationships between temperature seasonality, average temperature, age of the bivalve, length of the season, minimum growth temperatures and annual average and maximum growth rates. Values in green indicate strong correlations while values in red indicate the absence of a correlation. Data reported in **S14**.

The growing season is shorter than 365 days in all but five modelled years, demonstrating that growth stops or slowdowns did occur in *R. diluvianum*. Minimum growth temperatures (temperatures at which growth stops) are concentrated around 17°C (χ^2 = 0.0088; **Fig. 11a**) and correlate strongly to MAT (R^2=0.57; **Table 2**), suggesting that growth halts in *R. diluvianum* are not forced by an absolute temperature threshold, but rather by timing relative to the seasonality (circadian rhythm). If there would be a fixed temperature threshold (e.g. 6°C or 10°C for *Crassostrea gigas*; Lartaud et al., 2010; Ullmann et al., 2010) the length of the growth season should positively correlate with annual mean temperature, but this is not the case (R^2<0.1). Other authors have suggested growth in modern *C. gigas* does not actually cease completely but rather slows down significantly, which may also have been the case in *R. diluvianum*. On average, the moment of minimum growth in *R. diluvianum* occurs right after the highest temperatures of the year are reached (early autumn, **Fig. 9**).

The spawning season is concentrated in the two last months before the $\delta^{18}O$ maximum (first half of winter) when modelled water temperatures are ±17°C (**Fig. 11b**). Note that only three of the five shells allowed sampling of the first month of growth, and extrapolated records for the other two shells are likely unreliable. Comparing **Fig. 11a** and **Fig. 11b** shows that growth halts and spawning occur at similar temperatures (16.9 ± 0.7°C and 17.0 ± 0.3°C respectively, p = 0.72), suggesting that these events occur simultaneously or on either side of a seasonal growth halt (if it occurs). The timing of spawning in *R. diluvianum* differs from that in modern oysters, which generally spawn during the spring season, with the young oyster spat settling in in the summer (e.g. for *Crassostrea gigas*: Fan et al., 2011). In the case of modern oysters, it is known that reproduction requires a relatively warm minimum temperatures (ideally around 22°C for *C. gigas*; Cognie et al., 2006), and that a combination of salinity and temperature conditions is important (Fan et al., 2011), while extreme temperatures (>28°C; Surge et al., 2001) can induce shock. Perhaps the ideal conditions of *R. diluvianum* are lower (~17°C) or the ideal combination of temperature and salinity is met specifically in the autumn season.

751 **Figure 11b** shows that the distribution of months with fastest growth rate is random ($p(\chi^2) = 0.055$, <95%
752 confidence). However, in 27 of the 58 years, the growth peak occurs in the season with decreasing $\delta^{18}O$
753 values ("spring season"). **Table 2** shows that the extent of temperature seasonality (difference between
754 minimum and maximum $\delta^{18}O$ converted to temperature) significantly influences the length of the growing
755 season ($R^2 = 0.40$). However, total annual growth and maximum growth rates are independent of SST (both
756 seasonal extent and MAT) and ontogenetic age of the organism does not predict a significant part of any
757 of the above-mentioned growth and seasonality parameters (**Table 2**). If temperature controlled the growth
758 of *R. diluvianum* shells, larger temperature seasonality would increase the chance of crossing thresholds
759 of temperature tolerance which would shorten the length of the growing season. All this suggests that
760 temperature seasonality may not have been the dominant factor causing growth cessations in *R.*
761 *diluvianum*. This hypothesis is supported by the observation that temperatures at which growth cessations
762 occur (16.9 ± 0.7°C; **Fig. 11a**) show large variability and do not correspond significantly to the lowest
763 temperatures of the year.

764 These observations do not necessarily show that *R. diluvianum* tolerated larger temperature differences
765 than modern oyster taxa, because the extent of seasonality (14-25°C) causes neither the lower (~10°C)
766 nor the upper limit of temperature tolerance (~28°C) in modern oysters to be reached. If temperature
767 tolerance of *R. diluvianum* did resemble that of its closest modern relatives, then the mild seasonal
768 temperature cycle at Ivö Klack might have provided the ideal temperature range for its growth. Perhaps
769 these favorable conditions partly explain why biodiversity and abundance of invertebrates at Ivö Klack was
770 so high (Surlyk and Sørensen, 2010).

771 5.5.3 Productivity

772 Shell growth in *R. diluvianum* may not have been governed by temperature, but rather by changes in
773 productivity. The observation that peak growth rates and spawning both occur during the early spring
774 season (**Fig. 11b**) supports this hypothesis. Spring productivity blooms caused by increases in nutrient-rich
775 freshwater from onshore (Arthur et al., 1983; Krantz et al., 1987) or due to storm-induced mixing of more
776 nutrient-rich deeper waters are common in present-day mid- and high-latitude marine ecosystems (e.g.
777 Waniek, 2003; Danielsson et al., 2008). An increase in seasonal freshwater influx would cause longer

778 growth cessations to occur in the spring season, reducing the length of the growing season while also
779 dampening the reconstructed temperature seasonality (see **5.5.2**), which explains the correlation found
780 between these two parameters (**Table 2**). At the same time, this freshwater input would increase
781 reconstructed MAT by increasing $\delta^{18}O$ values in *R. diluvianum* shells, explaining the weak positive
782 correlation between MAT and length of the growing season (**Table 2**).

783 The occurrence of spring blooms is supported by weak 0.5-1.0‰ seasonal variability in $\delta^{13}C$ (**Fig. 6**).
784 Seasonal changes in productivity and/or salinity will cause changes in DIC in the environment, which are
785 apparent in the $\delta^{13}C$ of the shell above the ontogenetic trends and the effect of respiration on $\delta^{13}C$ (see **2.4**;
786 **Table 1**). The fact that a clear seasonality in $\delta^{13}C$ is absent from the stack in **Fig. 9** shows that these
787 productivity peaks do not occur at regular times of the season and that their effect on $\delta^{13}C$ is obscured by
788 ontogenetic trends. The 0.5-1.0‰ shifts in $\delta^{13}C$ that appear to be seasonal are much smaller than those in
789 modern oyster records (2-3‰ in low-latitude estuarine *Crassostrea virginica*; Surge et al., 2001; 2003;
790 Surge and Lohmann, 2008). Instead, the determined shifts more closely resemble the 0.5‰ variability in
791 $\delta^{13}C$ observed in modern *Crassostrea gigas* from the same approximate latitude as Ivö Klack in the North
792 Sea (Ullmann et al., 2013). The extreme isotopic shifts in the estuarine *C. virginica* specimens have been
793 shown to be caused by large shifts in freshwater input due to large seasonal variations in rainfall over
794 southern North America (Surge et al., 2003), while smaller variations in *C. gigas* from the North Sea are
795 produced by DIC changes due to seasonal changes in productivity (e.g. spring blooms; Ullmann et al.,
796 2013). The closer resemblance of *R. diluvianum* to the North Sea condition shows that the Ivö Klack
797 paleoenvironment did not experience large seasonal shifts in freshwater input and may have seen
798 productivity peaks in spring season. The latter interpretation is in agreement with the coincidence of
799 negative $\delta^{13}C$ excursions (in parts of the records not affected by ontogenetic trends and respiration) with
800 the low-$\delta^{18}O$ season (winter or spring; **Fig. 6**; **S6**) and the occurrence of spawning and a peak in growth
801 rates in the spring season (much like in wild modern oysters; Berthelin et al., 2000; **Fig. 9**; **Fig. 11a**).

802

803 5.5.4 Ontogeny

804 A part of the variation in $\delta^{13}C$ is explained by the presence of ontogenetic trends. These trends are known
805 to occur in marine and freshwater bivalves including in bivalves with symbionts (Klein et al., 1996b;
806 Watanabe et al., 2004; Gillikin et al., 2007; McConnaughey and Gillikin, 2008). The scale and direction of
807 the trends in $\delta^{13}C$ are not consistent between individual *R. diluvianum* shells, which is also the case in other
808 bivalve species (see **section 4.5**; **Table 1**; McConnaughey and Gillikin, 2008 and references therein).
809 Studies of modern bivalves show that in larger (older) bivalves, the contribution of respired CO_2 to carbon
810 in the shell is larger (up to 40%; Gillikin et al., 2007). This finding explains common trends of reducing $\delta^{13}C$
811 with age in bivalve shells, since respired carbon is isotopically lighter than environmental DIC. Since
812 ontogenetic trends are likely caused by changes in the amount of respired carbon entering the shell, and
813 the direction of these trends in *R. diluvianum*, the contribution of respired CO_2 to *R. diluvianum* shells likely
814 did not strictly increase with age. While this complicates the interpretation of $\delta^{13}C$ records, the relative
815 contribution of environmental changes to $\delta^{13}C$ variability in *R. diluvianum* shells does appear to be highest
816 on the positive end of the ontogenetic trend.

817

818 **5. Conclusions**

819 The highly biodiverse marine invertebrate community at Ivö Klack in the Kristianstad Basin in southern
820 Sweden offers a unique opportunity to recover a wealth of information about Campanian climate and
821 environment in high latitudes and the ecology and life of extinct invertebrate species that lived under these
822 conditions. The lack of burial and tectonic activity in the region favored *Rastellum diluvianum* fossil shells
823 from Ivö Klack to be well preserved, as is evident from the excellent preservation of growth structures typical
824 for ostreid shells as well as from limited evidence for geochemical changes associated with diagenetic
825 alteration. This excellent preservation allows the shells of *R. diluvianum* to be used to accurately and
826 precisely constrain the age of the Ivö Klack locality using strontium isotope stratigraphy (78.14 ± 0.26 Ma;
827 $^{87}Sr/^{86}Sr = 0.707552 \pm 0.000112$). Furthermore, *R. diluvianum* shells reveal sub-annual scale variability in
828 temperature, local environment and growth rates through a multi-proxy geochemical approach. The
829 combination of trace element and stable isotope measurements with growth modelling based on $\delta^{18}O$
830 records in the shells allow all measured proxies to be aligned on the same time axis. Application of transfer

functions for potential Mg/Ca, Mg/Li and Sr/Li temperature proxies established in modern invertebrates yields temperatures consistent with those calculated from $\delta^{18}O$ records. However, close examination of the seasonal phase relationships between these proxies reveals that the sub-annual variability in these trace element ratios is not controlled by temperature changes alone. This observation supports previous studies that found the expression of trace element proxies to be highly variable among species and even among different specimens of the same species. If trace element proxies are to be used for seasonality reconstructions in pre-Quaternary times, a more robust, non-species-specific model for the incorporation of trace elements by bivalves is required. Establishing such a model requires culture experiments with different bivalve species in which multiple parameters influencing trace element composition can be controlled (e.g. temperature, salinity, food intake and microstructure).

Stable isotope records in *R. diluvianum* shells reveal a MAT of 19°C with a seasonal water temperature range of ±11°C (14-25°C) at Ivö Klack. This value for MAT is lower than full marine SST of Boreal Chalk recently reevaluated with the clumped isotope thermometer. The difference highlights potential biases in temperature reconstructions based on $\delta^{18}O$ values and argue for reevaluations of these proxy records with more accurate techniques such as clumped isotope analysis. Comparing the seasonal temperature range reconstructed from *R. diluvianum* shells with other Late Cretaceous seasonality records from lower latitudes reveals that both latitudinal gradients and SST seasonality outside the tropics were much higher than predicted by climate models. This disagreement between data and models clearly illustrates the disadvantage of the lack of data on Late Cretaceous seasonality outside the (sub-)tropical latitudes and highlights how important such reconstructions are for improving our understanding of the dynamics in temperature variability in both space and time during greenhouse climates.

Finally, the coupled modelling and multi-proxy approach applied in this study sheds light on the effects of environmental changes on the life cycle and sub-annual growth of *R. diluvianum* shells. This study reveals that growth curves of *R. diluvianum* strongly resemble those in modern shallow marine bivalves that grow in coastal high latitude environments. However, changes in growth rate of our Boreal oysters seem unrelated to temperature, in contrast to modern, high-latitude oysters that tend to lower their growth rate and cease mineralization below a certain cold threshold. We conclude that growth cessations and sub-annual changes in growth rate in *R. diluvianum* were most likely not caused by intolerable temperatures,

but rather by circadian rhythm tied to the seasonal cycle and seasonal changes in sea surface productivity, driven by nutrient-rich freshwater inputs.

Acknowledgements

The authors would like to thank dr. Johan Vellekoop and dr. Andrew Johnson for their review that helped improve the manuscript, as well as editor dr Aninda Mazumdar for guiding the review process. This work was made possible with help of an IWT doctoral fellowship (IWT700) awarded to Niels de Winter. Instrumentation at the VUB was funded by Hercules infrastructure grants (HERC09 and HERC46). The authors acknowledge financial and logistic support from the Flemish Research Foundation (FWO, research project G017217N) and Teledyne CETAC Technologies (Omaha, NE, USA) as well as support from VUB Strategic Research (BAS48). Stijn Goolaerts is funded by a Belspo Brain project (BR/175/A2/CHICXULUB). Nicolas Thibault is funded by Carlsbergfondet grant CF16-0457. The authors would like to thank David Verstraeten for his help with stable isotope analyses. We thank Bart Lippens for assisting sample preparation and Joke Belza for help with the LA-ICP-MS analyses. Thanks are due to Julien Cilis (RBINS) for his assistance with SEM imaging. The authors wish to thank Emily Judd for discussions about her growth rate model for bivalve shells and Roger Barlow for his assistance with combining strontium isotope measurements with asymmetric error distributions.

Supplementary files

All supplementary files are stored in the open access online database Zenodo and can be accessed using the following link: https://doi.org/10.5281/zenodo.3699542

S1: High resolution (6400 dpi) scans of cross sections through the 12 shells of *Rastellum diluvianum* used in this study.

S2: Compilation of µXRF maps of cross sections through the 12 shells of *Rastellum diluvianum* used in this study.

S3: Compilation of XRF line scans measured through the foliated calcite of *Rastellum diluvianum* shells.

S4: Compilation of LA-ICP-MS data collected within the context of this study.

S5: Compilation of IRMS data used in this study.

S6: Composite figures of XRF linescan data through the shells of *Rastellum diluvianum*.

S7: Source code of the bivalve growth model adapted from Judd et al. (2018) including temperature equations for calcite.

S8: Compilation of strontium isotope data and ages used in this study.

S9: Compilation of the results from growth modelling on 5 *Rastellum diluvianum* shells.

S10: Compilation figures of proxy record data plotted on time axis for all 5 shells for which modelling was carried out.

S11: Plot of ontogenetic trends in $\delta^{13}C$ and Li/Ca proxies including statistics on the spread of the slopes of these trends.

S12: Data on trends in $\delta^{13}C$ and Li/Ca.

S13: Data used to create seasonality crossplots shown in **Fig. 7**.

S14: Data on statistics of the growth rates, seasonality and spawning season of all 5 bivalves for which modelling was done.

References

Al-Aasm, I. S. and Veizer, J.: Diagenetic stabilization of aragonite and low-Mg calcite, II. Stable isotopes in rudists, Journal of Sedimentary Research, 56(6), 763–770, 1986a.

Al-Aasm, I. S. and Veizer, J.: Diagenetic stabilization of aragonite and low-Mg calcite, I. Trace elements in rudists, Journal of Sedimentary Research, 56(1), 138–152, 1986.
Alberti, M., Fürsich, F. T., Abdelhady, A. A. and Andersen, N.: Middle to Late Jurassic equatorial seawater temperatures and latitudinal temperature gradients based on stable isotopes of brachiopods and oysters from Gebel Maghara, Egypt, Palaeogeography, Palaeoclimatology, Palaeoecology, 468, 301–313, doi:10.1016/j.palaeo.2016.11.052, 2017.
Amiot, R., Lécuyer, C., Buffetaut, E., Fluteau, F., Legendre, S. and Martineau, F.: Latitudinal temperature gradient during the Cretaceous Upper Campanian–Middle Maastrichtian: δ18O record of continental vertebrates, Earth and Planetary Science Letters, 226(1), 255–272, doi:10.1016/j.epsl.2004.07.015, 2004.
Andreasson, F. P. and Schmitz, B.: Winter and summer temperatures of the early middle Eocene of France from Turritella □18O profiles, , 4, 1996.
Arthur, M. A., Williams, D. F. and Jones, D. S.: Seasonal temperature-salinity changes and thermocline development in the mid-Atlantic Bight as recorded by the isotopic composition of bivalves, Geology, 11(11), 655–659, doi:10.1130/0091-7613(1983)11<655:STCATD>2.0.CO;2, 1983.
Bachelet, G.: Growth and recruitment of the tellinid bivalve Macoma balthica at the southern limit of its geographical distribution, the Gironde estuary (SW France), Marine Biology, 59(2), 105–117, 1980.
Barlow, R.: Asymmetric systematic errors, arXiv preprint physics/0306138, 2003.
Barrera, E. and Johnson, C. C.: Evolution of the Cretaceous Ocean-climate System, Geological Society of America., 1999.
Berthelin, C., Kellner, K. and Mathieu, M.: Storage metabolism in the Pacific oyster (Crassostrea gigas) in relation to summer mortalities and reproductive cycle (West Coast of France), Comparative Biochemistry and Physiology Part B: Biochemistry and Molecular Biology, 125(3), 359–369, doi:10.1016/S0305-0491(99)00187-X, 2000.
Brand, U. and Veizer, J.: Chemical diagenesis of a multicomponent carbonate system–1: Trace elements, Journal of Sedimentary Research, 50(4), 1219–1236, 1980.
Brand, U. and Veizer, J.: Chemical diagenesis of a multicomponent carbonate system-2: stable isotopes, Journal of Sedimentary Research, 51(3), 987–997, 1981.
Bryan, S. P. and Marchitto, T. M.: Mg/Ca–temperature proxy in benthic foraminifera: New calibrations from the Florida Straits and a hypothesis regarding Mg/Li, Paleoceanography, 23(2), PA2220, doi:10.1029/2007PA001553, 2008.
Burgener, L., Hyland, E., Huntington, K. W., Kelson, J. R. and Sewall, J. O.: Revisiting the equable climate problem during the Late Cretaceous greenhouse using paleosol carbonate clumped isotope temperatures from the Campanian of the Western Interior Basin, USA, Palaeogeography, Palaeoclimatology, Palaeoecology, 516, 244–267, doi:10.1016/j.palaeo.2018.12.004, 2018.
Butler, P. G., Wanamaker, A. D., Scourse, J. D., Richardson, C. A. and Reynolds, D. J.: Variability of marine climate on the North Icelandic Shelf in a 1357-year proxy archive based on growth increments in the bivalve Arctica islandica, Palaeogeography, Palaeoclimatology, Palaeoecology, 373, 141–151, doi:10.1016/j.palaeo.2012.01.016, 2013.
Carriker, M. R., Palmer, R. E. and Prezant, R. S.: Functional ultramorphology of the dissoconch valves of the oyster Crassostrea virginica, in Proceedings of the National Shellfisheries Association, vol. 70, pp. 139–183. [online] Available from: https://www.researchgate.net/profile/Robert_Prezant2/publication/236964411_Functional_ultramorphology_of_the_dissoconch_valves_of_the_oyster_Crassostrea_virginica/links/53dfd2260cf2a768e49be892.pdf, 1979.
Carriker, M. R., Swann, C. P., Prezant, R. S. and Counts, C. L.: Chemical elements in the aragonitic and calcitic microstructural groups of shell of the oysterCrassostrea virginica: A proton probe study, Marine Biology, 109(2), 287–297, 1991.
Christensen, W. K.: Upper Cretaceous belemnites from the Kristianstad area in Scania, Fossils and Strata., 1975.
Christensen, W. K.: The Albian to Maastrichtian of southern Sweden and Bornholm, Denmark: a review, Cretaceous Research, 5(4), 313–327, 1984.
Christensen, W. K.: Paleobiogeography and migration in the Late Cretaceous belemnite family Belemnitellidae, Acta palaeontologica polonica, 42(4), 457–495, 1997.
Clarke, L. J. and Jenkyns, H. C.: New oxygen isotope evidence for long-term Cretaceous climatic change in the Southern Hemisphere, Geology, 27(8), 699–702, 1999.
Cochran, J. K., Kallenberg, K., Landman, N. H., Harries, P. J., Weinreb, D., Turekian, K. K., Beck, A. J. and Cobban, W. A.: Effect of diagenesis on the Sr, O, and C isotope composition of late Cretaceous mollusks from the Western Interior Seaway of North America, American Journal of Science, 310(2), 69–88, doi:10.2475/02.2010.01, 2010.
Coggon, R. M., Teagle, D. A., Smith-Duque, C. E., Alt, J. C. and Cooper, M. J.: Reconstructing past seawater Mg/Ca and Sr/Ca from mid-ocean ridge flank calcium carbonate veins, Science, 327(5969), 1114–1117, 2010.
Cognie, B., Haure, J. and Barillé, L.: Spatial distribution in a temperate coastal ecosystem of the wild stock of the farmed oyster Crassostrea gigas (Thunberg), Aquaculture, 259(1–4), 249–259, 2006.
Csiki-Sava, Z., Buffetaut, E., Ősi, A., Pereda-Suberbiola, X. and Brusatte, S. L.: Island life in the Cretaceous - faunal composition, biogeography, evolution, and extinction of land-living vertebrates on the Late Cretaceous European archipelago, Zookeys, (469), 1–161, doi:10.3897/zookeys.469.8439, 2015.
Dalbeck, P., England, J., Cusack, M., Lee, M. R. and Fallick, A. E.: Crystallography and chemistry of the calcium carbonate polymorph switch in M. edulis shells, European Journal of Mineralogy, 18(5), 601–609, doi:10.1127/0935-1221/2006/0018-0601, 2006.
Danielsson, \AAsa, Papush, L. and Rahm, L.: Alterations in nutrient limitations—scenarios of a changing Baltic Sea, Journal of Marine Systems, 73(3–4), 263–283, 2008.
De Villiers, S.: Seawater strontium and Sr/Ca variability in the Atlantic and Pacific oceans, Earth and Planetary Science Letters, 171(4), 623–634, 1999.
DeConto, R. M., Hay, W. W., Thompson, S. L. and Bergengren, J.: Late Cretaceous climate and vegetation interactions: cold continental interior paradox, SPECIAL PAPERS-GEOLOGICAL SOCIETY OF AMERICA, 391–406, 1999.
Dellinger, M., West, A. J., Paris, G., Adkins, J. F., von Strandmann, P. A. P., Ullmann, C. V., Eagle, R. A., Freitas, P., Bagard, M.-L. and Ries, J. B.: The Li isotope composition of marine biogenic carbonates: Patterns and Mechanisms, Geochimica et Cosmochimica Acta, 236, 315–335, 2018.
Donnadieu, Y., Pucéat, E., Moiroud, M., Guillocheau, F. and Deconinck, J.-F.: A better-ventilated ocean triggered by Late Cretaceous changes in continental configuration, Nature Communications, 7, 10316, doi:10.1038/ncomms10316, 2016.

El Meknassi, S., Dera, G., Cardone, T., De Rafélis, M., Brahmi, C. and Chavagnac, V.: Sr isotope ratios of modern carbonate shells: Good and bad news for chemostratigraphy, Geology, 46(11), 1003–1006, 2018.
Fan, C., Koeniger, P., Wang, H. and Frechen, M.: Ligamental increments of the mid-Holocene Pacific oyster Crassostrea gigas are reliable independent proxies for seasonality in the western Bohai Sea, China, Palaeogeography, palaeoclimatology, palaeoecology, 299(3–4), 437–448, 2011.
Freitas, P. S., Clarke, L. J., Kennedy, H. A. and Richardson, C. A.: Inter-and intra-specimen variability masks reliable temperature control on shell Mg/Ca ratios in laboratory and field cultured Mytilus edulis and Pecten maximus (bivalvia), Biogeosciences Discussions, 5(1), 531–572, 2008.
Friedrich, O., Herrle, J. O. and Hemleben, C.: Climatic changes in the late Campanian—early Maastrichtian: Micropaleontological and stable isotopic evidence from an epicontinental sea, Journal of Foraminiferal Research, 35(3), 228–247, 2005.
Friedrich, O., Herrle, J. O., Wilson, P. A., Cooper, M. J., Erbacher, J. and Hemleben, C.: Early Maastrichtian carbon cycle perturbation and cooling event: Implications from the South Atlantic Ocean, Paleoceanography, 24(2), PA2211, doi:10.1029/2008PA001654, 2009.
Friedrich, O., Norris, R. D. and Erbacher, J.: Evolution of middle to Late Cretaceous oceans—a 55 my record of Earth's temperature and carbon cycle, Geology, 40(2), 107–110, 2012.
Füllenbach, C. S., Schöne, B. R. and Mertz-Kraus, R.: Strontium/lithium ratio in aragonitic shells of Cerastoderma edule (Bivalvia)—A new potential temperature proxy for brackish environments, Chemical Geology, 417, 341–355, 2015.
Galtsoff, P. S.: The American Oyster: US Fish and Wildlife Service, Fishery Bulletin, 64, 480, 1964.
Gillikin, D. P., Lorrain, A., Navez, J., Taylor, J. W., André, L., Keppens, E., Baeyens, W. and Dehairs, F.: Strong biological controls on Sr/Ca ratios in aragonitic marine bivalve shells, Geochemistry, Geophysics, Geosystems, 6(5), Q05009, 2005.
Gillikin, D. P., Lorrain, A., Bouillon, S., Willenz, P. and Dehairs, F.: Stable carbon isotopic composition of Mytilus edulis shells: relation to metabolism, salinity, δ 13 C DIC and phytoplankton, Organic Geochemistry, 37(10), 1371–1382, 2006.
Gillikin, D. P., Lorrain, A., Meng, L. and Dehairs, F.: A large metabolic carbon contribution to the δ 13 C record in marine aragonitic bivalve shells, Geochimica et Cosmochimica Acta, 71(12), 2936–2946, 2007.
Hart, D. R. and Chute, A. S.: Verification of Atlantic sea scallop (Placopecten magellanicus) shell growth rings by tracking cohorts in fishery closed areas, Canadian Journal of Fisheries and Aquatic Sciences, 66(5), 751–758, 2009.
Hay, W. W. and Floegel, S.: New thoughts about the Cretaceous climate and oceans, Earth-Science Reviews, 115(4), 262–272, 2012.
van Hinsbergen, D. J., de Groot, L. V., van Schaik, S. J., Spakman, W., Bijl, P. K., Sluijs, A., Langereis, C. G. and Brinkhuis, H.: A paleolatitude calculator for paleoclimate studies, PloS one, 10(6), e0126946, 2015.
Högdahl, K., Andersson, U. B. and Eklund, O.: The Transscandinavian Igneous Belt (TIB) in Sweden: a review of its character and evolution, Geological survey of Finland Espoo., 2004.
Huber, B. T., Norris, R. D. and MacLeod, K. G.: Deep-sea paleotemperature record of extreme warmth during the Cretaceous, Geology, 30(2), 123–126, 2002.
Huck, S., Heimhofer, U., Rameil, N., Bodin, S. and Immenhauser, A.: Strontium and carbon-isotope chronostratigraphy of Barremian–Aptian shoal-water carbonates: Northern Tethyan platform drowning predates OAE 1a, Earth and Planetary Science Letters, 304(3–4), 547–558, doi:10.1016/j.epsl.2011.02.031, 2011.
Huyghe, D., Lartaud, F., Emmanuel, L., Merle, D. and Renard, M.: Palaeogene climate evolution in the Paris Basin from oxygen stable isotope (δ18O) compositions of marine molluscs, Journal of the Geological Society, 172(5), 576–587, 2015.
Huyghe, D., de Rafelis, M., Ropert, M., Mouchi, V., Emmanuel, L., Renard, M. and Lartaud, F.: New insights into oyster high-resolution hinge growth patterns, Mar Biol, 166(4), 48, doi:10.1007/s00227-019-3496-2, 2019.
Immenhauser, A., Nägler, T. F., Steuber, T. and Hippler, D.: A critical assessment of mollusk 18 O/16 O, Mg/Ca, and 44 Ca/40 Ca ratios as proxies for Cretaceous seawater temperature seasonality, Palaeogeography, Palaeoclimatology, Palaeoecology, 215(3), 221–237, 2005.
IPCC: IPCC, 2013: Climate Change 2013: The Physical Science Basis. Contribution of Working Group I to the Fifth Assessment Report of the Intergovernmental Panel on Climate Change, 1535 pp, Cambridge Univ. Press, Cambridge, UK, and New York., 2013.
IRI/LDEO Climate Data Library URL http://iridl.ldeo.columbia.edu (accessed 06/03/20).
Ivany, L. C.: Reconstructing paleoseasonality from accretionary skeletal carbonates—challenges and opportunities, The Paleontological Society Papers, 18, 133–166, 2012.
Ivany, L. C. and Runnegar, B.: Early Permian seasonality from bivalve δ18O and implications for the oxygen isotopic composition of seawater, Geology, 38(11), 1027–1030, 2010.
Jablonski, D., Huang, S., Roy, K. and Valentine, J. W.: Shaping the latitudinal diversity gradient: new perspectives from a synthesis of paleobiology and biogeography, The American Naturalist, 189(1), 1–12, 2017.
Jarvis, I., Mabrouk, A., Moody, R. T. and de Cabrera, S.: Late Cretaceous (Campanian) carbon isotope events, sea-level change and correlation of the Tethyan and Boreal realms, Palaeogeography, Palaeoclimatology, Palaeoecology, 188(3), 215–248, 2002.
Jenkyns, H. C., Gale, A. S. and Corfield, R. M.: Carbon-and oxygen-isotope stratigraphy of the English Chalk and Italian Scaglia and its palaeoclimatic significance, Geological Magazine, 131(1), 1–34, 1994.
Jenkyns, H. C., Forster, A., Schouten, S. and Damsté, J. S. S.: High temperatures in the late Cretaceous Arctic Ocean, Nature, 432(7019), 888, 2004.
Jones, D. S.: Sclerochronology: reading the record of the molluscan shell: annual growth increments in the shells of bivalve molluscs record marine climatic changes and reveal surprising longevity, American Scientist, 71(4), 384–391, 1983.
Judd, E. J., Wilkinson, B. H. and Ivany, L. C.: The life and time of clams: Derivation of intra-annual growth rates from high-resolution oxygen isotope profiles, Palaeogeography, Palaeoclimatology, Palaeoecology, 490, 70–83, 2018.
Kawaguchi, T. and Watabe, N.: The organic matrices of the shell of the American oyster Crassostrea virginica Gmelin, Journal of Experimental Marine Biology and Ecology, 170(1), 11–28, doi:10.1016/0022-0981(93)90126-9, 1993.
Kim, S.-T. and O'Neil, J. R.: Equilibrium and nonequilibrium oxygen isotope effects in synthetic carbonates, Geochimica et Cosmochimica Acta, 61(16), 3461–3475, 1997.

Klein, R. T., Lohmann, K. C. and Thayer, C. W.: Bivalve skeletons record sea-surface temperature and δ18O via Mg/Ca and 18O/16O ratios, Geology, 24(5), 415–418, 1996a.
Klein, R. T., Lohmann, K. C. and Thayer, C. W.: SrCa and 13C12C ratios in skeletal calcite of Mytilus trossulus: Covariation with metabolic rate, salinity, and carbon isotopic composition of seawater, Geochimica et Cosmochimica Acta, 60(21), 4207–4221, doi:10.1016/S0016-7037(96)00232-3, 1996b.
Kominz, M. A., Browning, J. V., Miller, K. G., Sugarman, P. J., Mizintseva, S. and Scotese, C. R.: Late Cretaceous to Miocene sea-level estimates from the New Jersey and Delaware coastal plain coreholes: an error analysis, Basin Research, 20(2), 211–226, 2008.
Krantz, D. E., Williams, D. F. and Jones, D. S.: Ecological and paleoenvironmental information using stable isotope profiles from living and fossil molluscs, Palaeogeography, Palaeoclimatology, Palaeoecology, 58(3), 249–266, doi:10.1016/0031-0182(87)90064-2, 1987.
Kuznetsov, A. B., Semikhatov, M. A. and Gorokhov, I. M.: The Sr isotope composition of the world ocean, marginal and inland seas: Implications for the Sr isotope stratigraphy, Stratigr. Geol. Correl., 20(6), 501–515, doi:10.1134/S0869593812060044, 2012.
Lartaud, F., Emmanuel, L., De Rafélis, M., Ropert, M., Labourdette, N., Richardson, C. A. and Renard, M.: A latitudinal gradient of seasonal temperature variation recorded in oyster shells from the coastal waters of France and The Netherlands, Facies, 56(1), 13, 2010.
Lear, C. H., Elderfield, H. and Wilson, P. A.: A Cenozoic seawater Sr/Ca record from benthic foraminiferal calcite and its application in determining global weathering fluxes, Earth and Planetary Science Letters, 208(1), 69–84, doi:10.1016/S0012-821X(02)01156-1, 2003.
Li, Y., Qin, J. G., Abbott, C. A., Li, X. and Benkendorff, K.: Synergistic impacts of heat shock and spawning on the physiology and immune health of Crassostrea gigas: an explanation for summer mortality in Pacific oysters, American Journal of Physiology-Regulatory, Integrative and Comparative Physiology, 293(6), R2353–R2362, 2007.
Locarnini, R. A., Mishonov, A. V., Antonov, J. I., Boyer, T. P., Garcia, H. E., Baranova, O. K., Zweng, M. M., Paver, C. R., Reagan, J. R., Johnson, D. R., Hamilton, M. and Seidov, D.: World ocean atlas 2013. Volume 1, Temperature, U.S. Department of Commerce, National Oceanic and Atmospheric Administration, National Environmental Satellite, Data and Information Service, doi:10.7289/v55x26vd, 2013.
Lorrain, A., Paulet, Y.-M., Chauvaud, L., Dunbar, R., Mucciarone, D. and Fontugne, M.: δ 13 C variation in scallop shells: increasing metabolic carbon contribution with body size?, Geochimica et Cosmochimica Acta, 68(17), 3509–3519, 2004.
Lorrain, A., Gillikin, D. P., Paulet, Y.-M., Chauvaud, L., Le Mercier, A., Navez, J. and André, L.: Strong kinetic effects on Sr/Ca ratios in the calcitic bivalve Pecten maximus, Geology, 33(12), 965–968, 2005.
Lowenstam, H. A. and Epstein, S.: Paleotemperatures of the post-Aptian Cretaceous as determined by the oxygen isotope method, The Journal of Geology, 62(3), 207–248, 1954.
MacDonald, B. A. and Thompson, R. J.: Influence of temperature and food availability on the ecological energetics of the giant scallop Placopecten magellanicus. I. Growth rates of shell and somatic tissue., Marine ecology progress series. Oldendorf, 25(3), 279–294, 1985.
McArthur, J. M., Howarth, R. J. and Bailey, T. R.: Strontium Isotope Stratigraphy: LOWESS Version 3: Best Fit to the Marine Sr-Isotope Curve for 0–509 Ma and Accompanying Look-up Table for Deriving Numerical Age, The Journal of Geology, 109(2), 155–170, doi:10.1086/319243, 2001.
McArthur, J. M., Steuber, T., Page, K. N. and Landman, N. H.: Sr-isotope stratigraphy: assigning time in the Campanian, Pliensbachian, Toarcian, and Valanginian, The Journal of Geology, 124(5), 569–586, 2016.
McConnaughey, T. A.: Sub-equilibrium oxygen-18 and carbon-13 levels in biological carbonates: carbonate and kinetic models, Coral Reefs, 22(4), 316–327, 2003.
McConnaughey, T. A. and Gillikin, D. P.: Carbon isotopes in mollusk shell carbonates, Geo-Marine Letters, 28(5–6), 287–299, doi:10.1007/s00367-008-0116-4, 2008.
McConnaughey, T. A., Burdett, J., Whelan, J. F. and Paull, C. K.: Carbon isotopes in biological carbonates: respiration and photosynthesis, Geochimica et Cosmochimica Acta, 61(3), 611–622, 1997.
Meyers, S. R. and Malinverno, A.: Proterozoic Milankovitch cycles and the history of the solar system, PNAS, 201717689, doi:10.1073/pnas.1717689115, 2018.
Miller, K. G., Wright, J. D. and Browning, J. V.: Visions of ice sheets in a greenhouse world, Marine Geology, 217(3), 215–231, doi:10.1016/j.margeo.2005.02.007, 2005.
Montgomery, P., Hailwood, E. A., Gale, A. S. and Burnett, J. A.: The magnetostratigraphy of Coniacian-Late Campanian chalk sequences in southern England, Earth and Planetary Science Letters, 156(3), 209–224, doi:10.1016/S0012-821X(98)00008-9, 1998.
Mook, W. G.: Paleotemperatures and chlorinities from stable carbon and oxygen isotopes in shell carbonate, Palaeogeography, Palaeoclimatology, Palaeoecology, 9(4), 245–263, doi:10.1016/0031-0182(71)90002-2, 1971.
Mouchi, V., De Rafélis, M., Lartaud, F., Fialin, M. and Verrecchia, E.: Chemical labelling of oyster shells used for time-calibrated high-resolution Mg/Ca ratios: a tool for estimation of past seasonal temperature variations, Palaeogeography, Palaeoclimatology, Palaeoecology, 373, 66–74, 2013.
NOAA Earth System Research Laboratory: NOAA Optimum Interpolation (IO) Sea Surface Temperature (SST) http://www.esrl.noaa.gov/psd/data/gridded/data.noaa.oisst.v2.html (accessed 01/21/19).
O'Brien, C. L., Robinson, S. A., Pancost, R. D., Sinninghe Damsté, J. S., Schouten, S., Lunt, D. J., Alsenz, H., Bornemann, A., Bottini, C., Brassell, S. C., Farnsworth, A., Forster, A., Huber, B. T., Inglis, G. N., Jenkyns, H. C., Linnert, C., Littler, K., Markwick, P., McAnena, A., Mutterlose, J., Naafs, B. D. A., Püttmann, W., Sluijs, A., van Helmond, N. A. G. M., Vellekoop, J., Wagner, T. and Wrobel, N. E.: Cretaceous sea-surface temperature evolution: Constraints from TEX 86 and planktonic foraminiferal oxygen isotopes, Earth-Science Reviews, 172, 224–247, doi:10.1016/j.earscirev.2017.07.012, 2017.
Ogg, J. G., Ogg, G. and Gradstein, F. M.: A concise geologic time scale: 2016, Elsevier., 2016.
Palmer, R. E. and Carriker, M. R.: Effects of cultural conditions on morphology of the shell of the oyster Crassostrea virginica, in Proceedings of the National Shellfisheries Association, vol. 69, pp. 58–72., 1979.
Pearson, P. N., Ditchfield, P. W., Singano, J., Harcourt-Brown, K. G., Nicholas, C. J., Olsson, R. K., Shackleton, N. J. and Hall, M. A.: Warm tropical sea surface temperatures in the Late Cretaceous and Eocene epochs, Nature, 413(6855), 481, 2001.

Perdiou, A., Thibault, N., Anderskouv, K., Van Buchem, F., Buijs, G. J. A. and Bjerrum, C. J.: Orbital calibration of the late Campanian carbon isotope event in the North Sea, Journal of the Geological Society, 173(3), 504–517, 2016.
Prandle, D. and Lane, A.: The annual temperature cycle in shelf seas, Continental Shelf Research, 15(6), 681–704, doi:10.1016/0278-4343(94)E0029-L, 1995.
Rausch, S., Böhm, F., Bach, W., Klügel, A. and Eisenhauer, A.: Calcium carbonate veins in ocean crust record a threefold increase of seawater Mg/Ca in the past 30 million years, Earth and Planetary Science Letters, 362, 215–224, 2013.
Rayner, N. A., Parker, D. E., Horton, E. B., Folland, C. K., Alexander, L. V., Rowell, D. P., Kent, E. C. and Kaplan, A.: Global analyses of sea surface temperature, sea ice, and night marine air temperature since the late nineteenth century, Journal of Geophysical Research: Atmospheres, 108(D14), doi:10.1029/2002JD002670, 2003.
Reid, R. E. H.: The Chalk Sea, The Irish Naturalists' Journal, 17(11), 357–375, 1973.
Richardson, C. A., Peharda, M., Kennedy, H., Kennedy, P. and Onofri, V.: Age, growth rate and season of recruitment of Pinna nobilis (L) in the Croatian Adriatic determined from Mg: Ca and Sr: Ca shell profiles, Journal of Experimental Marine Biology and Ecology, 299(1), 1–16, 2004.
Roy, K., Jablonski, D. and Martien, K. K.: Invariant size–frequency distributions along a latitudinal gradient in marine bivalves, PNAS, 97(24), 13150–13155, doi:10.1073/pnas.97.24.13150, 2000.
Rucker, J. B. and Valentine, J. W.: Salinity Response of Trace Element Concentration in Crassostrea virginica, Nature, 190(4781), 1099–1100, doi:10.1038/1901099a0, 1961.
Sano, Y., Kobayashi, S., Shirai, K., Takahata, N., Matsumoto, K., Watanabe, T., Sowa, K. and Iwai, K.: Past daily light cycle recorded in the strontium/calcium ratios of giant clam shells, Nat Commun, 3, 761, doi:10.1038/ncomms1763, 2012.
Schöne, B. R. and Gillikin, D. P.: Unraveling environmental histories from skeletal diaries — Advances in sclerochronology, Palaeogeography, Palaeoclimatology, Palaeoecology, 373, 1–5, doi:10.1016/j.palaeo.2012.11.026, 2013.
SCHÖNE, B. R., Houk, S. D., FREYRE CASTRO, A. D., Fiebig, J., Oschmann, W., KRÖNCKE, I., Dreyer, W. and Gosselck, F.: Daily growth rates in shells of Arctica islandica: assessing sub-seasonal environmental controls on a long-lived bivalve mollusk, Palaios, 20(1), 78–92, 2005.
Schöne, B. R., Zhang, Z., Jacob, D., Gillikin, D. P., Tütken, T., Garbe-Schönberg, D., McConnaughey, T. and Soldati, A.: Effect of organic matrices on the determination of the trace element chemistry (Mg, Sr, Mg/Ca, Sr/Ca) of aragonitic bivalve shells (Arctica islandica)—Comparison of ICP-OES and LA-ICP-MS data, Geochemical Journal, 44(1), 23–37, 2010.
Schöne, B. R., Zhang, Z., Radermacher, P., Thébault, J., Jacob, D. E., Nunn, E. V. and Maurer, A.-F.: Sr/Ca and Mg/Ca ratios of ontogenetically old, long-lived bivalve shells (Arctica islandica) and their function as paleotemperature proxies, Palaeogeography, Palaeoclimatology, Palaeoecology, 302(1), 52–64, 2011.
Schöne, B. R., Radermacher, P., Zhang, Z. and Jacob, D. E.: Crystal fabrics and element impurities (Sr/Ca, Mg/Ca, and Ba/Ca) in shells of Arctica islandica—Implications for paleoclimate reconstructions, Palaeogeography, Palaeoclimatology, Palaeoecology, 373, 50–59, 2013.
Scotese, C.: A NEW GLOBAL TEMPERATURE CURVE FOR THE PHANEROZOIC., 2016.
Shackleton, N. J.: Paleogene stable isotope events, Palaeogeography, Palaeoclimatology, Palaeoecology, 57(1), 91–102, 1986.
Snoeck, C., Lee-Thorp, J., Schulting, R., Jong, J., Debouge, W. and Mattielli, N.: Calcined bone provides a reliable substrate for strontium isotope ratios as shown by an enrichment experiment, Rapid communications in mass spectrometry, 29(1), 107–114, 2015.
Sørensen, A. M., Surlyk, F. and Jagt, J. W. M.: Adaptive morphologies and guild structure in a high-diversity bivalve fauna from an early Campanian rocky shore, Ivö Klack (Sweden), Cretaceous Research, 33(1), 21–41, doi:10.1016/j.cretres.2011.07.004, 2012.
Sørensen, A. M., Ullmann, C. V., Thibault, N. and Korte, C.: Geochemical signatures of the early Campanian belemnite Belemnellocamax mammillatus from the Kristianstad Basin in Scania, Sweden, Palaeogeography, palaeoclimatology, palaeoecology, 433, 191–200, 2015.
Stanley, S. M. and Hardie, L. A.: Secular oscillations in the carbonate mineralogy of reef-building and sediment-producing organisms driven by tectonically forced shifts in seawater chemistry, Palaeogeography, Palaeoclimatology, Palaeoecology, 144(1), 3–19, 1998.
Stenzel, H. B.: Aragonite and calcite as constituents of adult oyster shells, Science, 142(3589), 232–233, 1963.
Steuber, T.: Isotopic and chemical intra-shell variations in low-Mg calcite of rudist bivalves (Mollusca-Hippuritacea): disequilibrium fractionations and late Cretaceous seasonality, International Journal of Earth Sciences, 88(3), 551–570, 1999.
Steuber, T., Rauch, M., Masse, J.-P., Graaf, J. and Malkoč, M.: Low-latitude seasonality of Cretaceous temperatures in warm and cold episodes, Nature, 437(7063), 1341–1344, 2005.
Strahl, J., Philipp, E., Brey, T., Broeg, K. and Abele, D.: Physiological aging in the Icelandic population of the ocean quahog Arctica islandica, Aquatic Biology, 1(1), 77–83, 2007.
Surge, D. and Lohmann, K. C.: Evaluating Mg/Ca ratios as a temperature proxy in the estuarine oyster, Crassostrea virginica, Journal of Geophysical Research: Biogeosciences, 113(G2) [online] Available from: http://onlinelibrary.wiley.com/doi/10.1029/2007JG000623/full (Accessed 28 November 2016), 2008.
Surge, D., Lohmann, K. C. and Dettman, D. L.: Controls on isotopic chemistry of the American oyster, Crassostrea virginica: implications for growth patterns, Palaeogeography, Palaeoclimatology, Palaeoecology, 172(3), 283–296, 2001.
Surge, D. M., Lohmann, K. C. and Goodfriend, G. A.: Reconstructing estuarine conditions: oyster shells as recorders of environmental change, Southwest Florida, Estuarine, Coastal and Shelf Science, 57(5), 737–756, doi:10.1016/S0272-7714(02)00370-0, 2003.
Surlyk, F. and Christensen, W. K.: Epifaunal zonation on an Upper Cretaceous rocky coast, Geology, 2(11), 529–534, 1974.
Surlyk, F. and Sørensen, A. M.: An early Campanian rocky shore at Ivö Klack, southern Sweden, Cretaceous Research, 31(6), 567–576, 2010.
Tagliavento, M., John, C. M. and Stemmerik, L.: Tropical temperature in the Maastrichtian Danish Basin: Data from coccolith Δ47 and δ18O, Geology, 47(11), 1074–1078, 2019.
Thibault, N., Husson, D., Harlou, R., Gardin, S., Galbrun, B., Huret, E. and Minoletti, F.: Astronomical calibration of upper Campanian–Maastrichtian carbon isotope events and calcareous plankton biostratigraphy in the Indian Ocean (ODP Hole

762C): Implication for the age of the Campanian–Maastrichtian boundary, Palaeogeography, Palaeoclimatology, Palaeoecology, 337–338, 52–71, doi:10.1016/j.palaeo.2012.03.027, 2012.
Thibault, N., Harlou, R., Schovsbo, N. H., Stemmerik, L. and Surlyk, F.: Late Cretaceous (late Campanian–Maastrichtian) sea-surface temperature record of the Boreal Chalk Sea, Climate of the Past, 12(2), 429–438, 2016.
Uchikawa, J. and Zeebe, R. E.: The effect of carbonic anhydrase on the kinetics and equilibrium of the oxygen isotope exchange in the CO2–H2O system: Implications for δ18O vital effects in biogenic carbonates, Geochimica et Cosmochimica Acta, 95, 15–34, 2012.
Ullmann, C. V. and Korte, C.: Diagenetic alteration in low-Mg calcite from macrofossils: a review, Geological Quarterly, 59(1), 3–20, 2015.
Ullmann, C. V., Wiechert, U. and Korte, C.: Oxygen isotope fluctuations in a modern North Sea oyster (Crassostrea gigas) compared with annual variations in seawater temperature: Implications for palaeoclimate studies, Chemical Geology, 277(1), 160–166, 2010.
Ullmann, C. V., Böhm, F., Rickaby, R. E., Wiechert, U. and Korte, C.: The Giant Pacific Oyster (Crassostrea gigas) as a modern analog for fossil ostreoids: isotopic (Ca, O, C) and elemental (Mg/Ca, Sr/Ca, Mn/Ca) proxies, Geochemistry, Geophysics, Geosystems, 14(10), 4109–4120, 2013.
Upchurch Jr, G. R., Kiehl, J., Shields, C., Scherer, J. and Scotese, C.: Latitudinal temperature gradients and high-latitude temperatures during the latest Cretaceous: Congruence of geologic data and climate models, Geology, 43(8), 683–686, 2015.
Vansteenberge, S., de Winter, N. J., Sinnesael, M., Xueqin, Z., Verheyden, S. and Claeys, P.: Benchtop µXRF as a tool for speleothem trace elemental analysis: Validation, limitations and application on an Eemian to early Weichselian (125–97 ka) stalagmite from Belgium, Palaeogeography, Palaeoclimatology, Palaeoecology, 538, 109460, doi:10.1016/j.palaeo.2019.109460, 2020.
Veizer, J.: Chemical diagenesis of carbonates: theory and application of trace element technique, [online] Available from: http://archives.datapages.com/data/sepm_sp/SC10/Chemical_Diagenesis.htm, 1983.
Veizer, J. and Prokoph, A.: Temperatures and oxygen isotopic composition of Phanerozoic oceans, Earth-Science Reviews, 146, 92–104, 2015.
Voigt, S. and Schönfeld, J.: Cyclostratigraphy of the reference section for the Cretaceous white chalk of northern Germany, Lägerdorf–Kronsmoor: A late Campanian–early Maastrichtian orbital time scale, Palaeogeography, Palaeoclimatology, Palaeoecology, 287(1), 67–80, doi:10.1016/j.palaeo.2010.01.017, 2010.
Voigt, S., Friedrich, O., Norris, R. D. and Schönfeld, J.: Campanian–Maastrichtian carbon isotope stratigraphy: shelf-ocean correlation between the European shelf sea and the tropical Pacific Ocean, Newsletters on Stratigraphy, 44(1), 57–72, 2010.
Von Bertalanffy, L.: Quantitative laws in metabolism and growth, The quarterly review of biology, 32(3), 217–231, 1957.
Wagreich, M., Hohenegger, J. and Neuhuber, S.: Nannofossil biostratigraphy, strontium and carbon isotope stratigraphy, cyclostratigraphy and an astronomically calibrated duration of the Late Campanian Radotruncana calcarata Zone, Cretaceous Research, 38, 80–96, 2012.
Waniek, J. J.: The role of physical forcing in initiation of spring blooms in the northeast Atlantic, Journal of Marine Systems, 39(1–2), 57–82, 2003.
Warter, V., Erez, J. and Müller, W.: Environmental and physiological controls on daily trace element incorporation in Tridacna crocea from combined laboratory culturing and ultra-high resolution LA-ICP-MS analysis, Palaeogeography, Palaeoclimatology, Palaeoecology, 496, 32–47, doi:10.1016/j.palaeo.2017.12.038, 2018.
Watanabe, T., Suzuki, A., Kawahata, H., Kan, H. and Ogawa, S.: A 60-year isotopic record from a mid-Holocene fossil giant clam (Tridacna gigas) in the Ryukyu Islands: physiological and paleoclimatic implications, Palaeogeography, Palaeoclimatology, Palaeoecology, 212(3–4), 343–354, 2004.
Weiner, S. and Dove, P. M.: An overview of biomineralization processes and the problem of the vital effect, Reviews in mineralogy and geochemistry, 54(1), 1–29, 2003.
Weis, D., Kieffer, B., Maerschalk, C., Barling, J., Jong, J. de, Williams, G. A., Hanano, D., Pretorius, W., Mattielli, N., Scoates, J. S., Goolaerts, A., Friedman, R. M. and Mahoney, J. B.: High-precision isotopic characterization of USGS reference materials by TIMS and MC-ICP-MS, Geochemistry, Geophysics, Geosystems, 7(8), Q08006, doi:10.1029/2006GC001283, 2006.
Wendler, I.: A critical evaluation of carbon isotope stratigraphy and biostratigraphic implications for Late Cretaceous global correlation, Earth-Science Reviews, 126, 116–146, doi:10.1016/j.earscirev.2013.08.003, 2013.
de Winter, N. J. and Claeys, P.: Micro X-ray fluorescence (µXRF) line scanning on Cretaceous rudist bivalves: A new method for reproducible trace element profiles in bivalve calcite, edited by M. R. Petrizzo, Sedimentology, 64(1), 231–251, doi:10.1111/sed.12299, 2016.
de Winter, N. J., Sinnesael, M., Makarona, C., Vansteenberge, S. and Claeys, P.: Trace element analyses of carbonates using portable and micro-X-ray fluorescence: performance and optimization of measurement parameters and strategies, Journal of Analytical Atomic Spectrometry, 32(6), 1211–1223, 2017b.
de Winter, N. J., Goderis, S., Dehairs, F., Jagt, J. W., Fraaije, R. H., Van Malderen, S. J., Vanhaecke, F. and Claeys, P.: Tropical seasonality in the late Campanian (late Cretaceous): Comparison between multiproxy records from three bivalve taxa from Oman, Palaeogeography, Palaeoclimatology, Palaeoecology, 485, 740–760, 2017a.
de Winter, N. J., Vellekoop, J., Vorsselmans, R., Golreihan, A., Soete, J., Petersen, S. V., Meyer, K. W., Casadio, S., Speijer, R. P. and Claeys, P.: An assessment of latest Cretaceous Pycnodonte vesicularis (Lamarck, 1806) shells as records for palaeoseasonality: a multi-proxy investigation, Climate of the Past, 14(6), 725–749, 2018.
de Winter, N. J., Goderis, S., Malderen, S. J. M. V., Sinnesael, M., Vansteenberge, S., Snoeck, C., Belza, J., Vanhaecke, F. and Claeys, P.: Subdaily-Scale Chemical Variability in a Torreites Sanchezi Rudist Shell: Implications for Rudist Paleobiology and the Cretaceous Day-Night Cycle, Paleoceanography and Paleoclimatology, 35(2), e2019PA003723, doi:10.1029/2019PA003723, 2020a.
de Winter, N. J., Vellekoop, J., Clark, A. J., Stassen, P., Speijer, R. P. and Claeys, P.: The giant marine gastropod Campanile giganteum (Lamarck, 1804) as a high-resolution archive of seasonality in the Eocene greenhouse world, Geochemistry, Geophysics, Geosystems, n/a(n/a), e2019GC008794, doi:10.1029/2019GC008794, 2020b.

Yang, D., Huang, Y., Guo, W., Huang, Q., Ren, Y. and Wang, C.: Late Santonian-early Campanian lake-level fluctuations in the Songliao Basin, NE China and their relationship to coeval eustatic changes, Cretaceous Research, 92, 138–149, doi:10.1016/j.cretres.2018.07.008, 2018.

Yoshimura, T., Tanimizu, M., Inoue, M., Suzuki, A., Iwasaki, N. and Kawahata, H.: Mg isotope fractionation in biogenic carbonates of deep-sea coral, benthic foraminifera, and hermatypic coral, Anal Bioanal Chem, 401(9), 2755, doi:10.1007/s00216-011-5264-0, 2011.

Zimmt, J. B., Lockwood, R., Andrus, C. F. T. and Herbert, G. S.: Sclerochronological basis for growth band counting: A reliable technique for life-span determination of Crassostrea virginica from the mid-Atlantic United States, Palaeogeography, Palaeoclimatology, Palaeoecology, 516, 54–63, 2018.